Master's Thesis

Master in Telecommunication Engineering

Characterization and modeling of a coaxial cavity quadruplet based filter for mobile phone LTE-2 band

David Eslava Sabaté

Supervisor: Pedro de Paco Sánchez

Telecomunications Systems Department

Escola Tècnica Superior d'Enginyeria (ETSE)

Universitat Autònoma de Barcelona (UAB)

February 2016

UAB

El sotasignant, Pedro de Paco Sánchez, Professor de l'Escola Tècnica Superior d'Enginyeria (ETSE) de la Universitat Autònoma de Barcelona (UAB),

CERTIFICA:

Que el projecte presentat en aquesta memòria de Treball Final de Màster ha estat realitzat sota la seva direcció per l'alumne David Eslava Sabaté.

I, perquè consti a tots els efectes, signa el present certificat.

Bellaterra, Febrer del 2016

Signatura: Pedro de Paco Sánchez

Acknowledgments

The present work was possible tanks to many people who helped me during these last years, and hence this also belongs in part to them.

I would like to give special thanks to my supervisor, Prof. Pedro de Paco for placing his trust in me and give me the opportunity to work in such interesting fields of microwave engineering. As well, I would like to thank him and Alfred Gimenez their support, advices, teachings, help, availability and patience for resolving my questions.

Likewise I would like to thank my family and friends for their comprehension and affection during these years. Special thanks to Daniel Solans, Eduard Ametller, Núria Rama and my parents.

Contents

List of Figures

Chapter 1

MOTIVATIONS AND OBJECTIVES

Nowadays smartphone business domains the market and it is growing year after year. That's why lots of companies work against time in order to develop better, smaller and cheaper technologies to adapt to this market. In RF-MW engineering we face up the design of a lot of components for those technologies, one of the top, the filters. Not only used inside smartphones also in base stations.

Receive (Rx) Filters are used to eliminate the out of band signals prior to amplification by an LNA and down conversion by the base station.This project is aimed to ascertain, study and design a cavity filter with placed transmission zeros with similar characteristics to the commercial one.

In addition to the catalog standards, custom designs normally are generated to support specific customer requirements. Further customization through integrated solutions provides improved performance and reduced physical size while simplifying customer procurement. This means that being able to design a cavity filter for a determined band of frequency and concrete characteristics means being able to repeat and modify the process for almost any band and therefore have the ability to manufacture customized filters.

Main idea is to show and understand the design process of a generalized Chebyshev response filter. After that, develop a Matlab program that given a filter specifications by the user autocratically gives the filter parameters for design (polynomials, matrices, couplings...). And finally show how to implement those parameters on a real circuit in order to being able to manufacture a physical filter. Before manufacturing there is always a step of validation, and that is why in the final section of the final chapter of this project we will try to implement the designed filter in HFSS EM simulator and it would be nice to have it matching as much as possible with the real filter measurements, previously measured with a network analyzer.

In order to accomplish those objectives, some previous requirements are needed and also take part of the objectives:

- Knowing nodal filter representation and design methods of those filters as well as polynomials and coupling matrices design.

- Knowing coupled circuit filters structure and how to design them from previous calculated couplings.
- Knowing the optimum parameters of meshing and error in order to be able to compare filter simulation with measurements.

Finally, this project main objectives will be:

- Show and understand the design process of a generalized Chebyshev response filter.
- Develop a Matlab program that given a filter specifications by the user automatically gives the filter parameters for design.
- Implement the filter in coaxial cavity technology and try to simulate it with 3D HFSS simulator.

1.1 Memory structure

This memory is composed by 6 chapters, and they are structured this way:

Chapter 2. Filter introduction: Filters are introduced in general as well as its main characteristics and parameters of design. Then Chebyshev response is presented including an introduction to general Chebyshev response. The Chapter ends with a presentation of the filter of reference that will be tried to be designed.

Chapter 3. Synthesis of a general class of the Chebyshev filter function: characteristic polynomials for a lowpass filter network are are deeply explained, calculated and checked by calculating with them the transmission and reflection parameters and plotting them observing the persecuted response.

Chapter 4. Coupling matrix synthesis of filter networks: The calculation of coupling matrix from previously obtained characteristic polynomials is deeply explained and calculated. Finally re-configuration of the calculated matrix is explained and performed in order to adapt the matrix to the proper configuration we are going to implement the filter.

Chapter 5. Physical realization of the coupling matrix: Coaxial resonators technology is introduced. Then method to obtain the couplings calculated in previous chapter matrix with coaxial resonator is explained and applied. The chapter ends with an introduction to HFSS meshing critical points and an explanation of steps to simulate the filter in HFSS.

Chapter 6. Conclusions: This chapter closes the project highlighting the main results obtained during the realization of it and proposing future work.

Chapter 2

FILTER INTRODUCTION

Filters are key elements in all communications devices. A filter is a two-port device, whose main mission is to select / reject a particular frequency band wanted / unwanted. That's why there are different types of filters, depending on the frequency bands that wish to eliminate, mitigate or select. We can classify them in terms of their function in four categories: low pass, high pass, band pass and stop band.

Because of the goals of this project in this chapter are presented the bandpass filters. In[1] and[2] you can find all the necessary information for a more complete version of the filters here mentioned.

Bandpass filters serve a variety of functions in communication, radar and instrumentation subsystems. Of the available techniques for the design of bandpass filters, those techniques based upon the low pass elements of a prototype filter have yielded successful results in a wide range of applications. The low pass prototype elements are the normalized values of the circuit components of a filter that have been synthesized for a unique passband response, and in some cases, a unique out-of-band response. The low pass prototype elements are available to the designer in a number of tabulated sources and are generally given in a normalized format, that is, mathematically related to a parameter of the filter prototype.

LOW PASS PROTOTYPE FILTERS

In communications systems, filter networks are required to transmit and attenuate signals in specified frequency bands. Ideally, this must be accomplished with the minimum of distortion and loss of energy of the transmitted signal. The synthesis of filter networks is carried out by developing lumped lossless lowpass filters that are normalized in terms of frequency and impedance, and terminated in resistors of equal value. By scaling in frequency and amplitude, it is then possible to derive filter networks over any desired frequency range and impedance levels. This simplifies the design of practical filters regardless of their frequency range and how they are realized physically. The lowpass prototype filter is normalized to a cutoff frequency of 1 radian per second and terminated in resistors of 1 Ohm.

Low pass prototype filters are lumped element networks that have been synthesized to provide a desired filter transfer function. The element values have been normalized with respect to one or more filter design parameters (cutoff frequency, for example) to offer the greatest flexibility, ease of use and tabulation. The elements of the low pass prototype filter are the capacitors and inductors of the ladder networks of the synthesized filter networks as shown in Figure 2.1.

The two possible implementations of the low pass prototype filter topologies. In both cases, the network transfer function is

$$T(s) = \frac{e_2(s)}{e_1(s)} \tag{2.1}$$

where $s = \sigma + j\omega$, the Laplace complex frequency variable.

Clearly, the transfer function, T(s), is a polynomial of order n, where n is the number of elements of the low pass filter prototype. The illustrated circuit topologies represent a filter prototype containing an odd number of circuit elements. To represent an even number of elements of the prototype filter, simply remove the last capacitor or inductor of the ladder network.

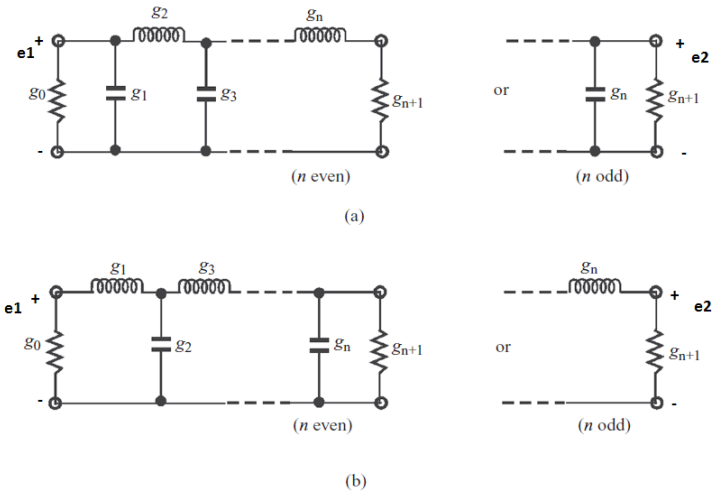

Figure 2.1: Circuit topologies of low pass prototype filters.

RESPONSE TYPE

Butterworth and Chebyshev responses are the most common response types. With Butterworth one, the response is a flat in the passband but has less abrupt transition band. However, the Chebyshev response has a certain ripple in the pass band, but the transition band is more abrupt. In the case of Figure 2.2, represents a 3 dB Chebyshev ripple, so the cutoff frequency matches a -3 dB gain, although it is not always necessarily this way. For instance, if the ripple was 0.1 dB, cutoff frequency would be at -0.1 dB.

For a lowpass filter, the number of peaks is n / 2 where n is the order of the filter. Therefore, from Figure 2.2, one could infer that it is a filter of fourth order.

ORDER

The number of reactive elements is determined by the order of the filter, n. The more the order, the better the answer at expenses of increasing cost and size. The order is determined by the attenuation needed at a certain frequency, L_{AS}. If this frequency is close to the passband and high attenuation is required, the minimum order required will be greater. This is determined by the equation 2.2 for Chebyshev and equation 2.3 to Butterworth.

$$n \geq \frac{cosh^{-1}\sqrt{\frac{10^{0.1L_{AS}}-1}{10^{0.1L_{AR}-1}}}}{cosh^{-1}\Omega_s} \tag{2.2}$$

where L_{AR}(dB) is the ripple in the passband and L_{AS}(dB) is the minimum stopband attenuation.

$$n \geq \frac{log(10^{0.1L_{AS}}-1)}{2log(\Omega_s)} \tag{2.3}$$

RETURN LOSS, RL

Another important factor to take into account the design of filters are the return loss, which are the power losses experienced by the signal due to the reflection and return part of it. It is usually expressed in dB:

$$RL(dB) = 10log_{10}\frac{P_i}{P_R} = 10log_{10}S_{11} \tag{2.4}$$

So, this parameter gives an idea about the filter's quality level in the passband. The more RL the more transmission in passband.

INSERTION LOSS, IL

It is defined as the loss of signal strength resulting from the insertion of a device in a transmission line and is usually expressed in dB:

$$IL(dB) = 10log_{10}\frac{P_T}{P_R} = 10log_{10}S_{21} \tag{2.5}$$

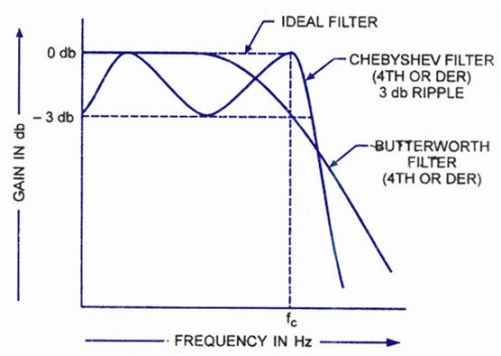

Figure 2.2: Chevyshev and Butterworth lowpass typical transmission response.

2.1 Chebyshev Response

Because we cannot have a zero loss over the entire passband without violating the causality condition[a], it is only possible to have a zero loss at a finite number of frequencies. Such frequencies are referred to as reflection zeros, for which no power is reflected. An obvious consequence of this is that all the reflection zeros of the filter function are confined to the passband, as shows Figure 3.3. Furthermore, the magnitude of the maximum reflected power over the passband (Return Loss) serves as a design parameter.

For purposes of illustration, an example representing a Chebyshev filter is offered. The power transfer function of the Chebyshev filter may be represented by

$$T(f') = 10log\{1+\varepsilon cos^2[ncos^{-1}(f')]\}\ for\ f' \leq 1.0 \tag{2.6}$$

$$T(f') = 10log\{1+\varepsilon cosh^2[ncosh^{-1}(f')]\}\ for\ f' \geq 1.0 \tag{2.7}$$

and

$$\varepsilon = log^{-1}\left(\frac{L_{AR}}{10}\right) - 1 \tag{2.8}$$

These equations represent the power transfer function of the Chebyshev low pass prototype filter with normalized filter cutoff frequency f' of 1.0 Hz.

To construct the filter at another frequency (1.0 GHz, for example) and circuit impedance level ($R_0 = 50\Omega$), the element values must be adjusted (de-normalized) in accordance with

[a]All filter functions that are described by a ratio of polynomials are causal. This math function can be decomposed to a sum of fractions as in partial fraction expansion. Then the Laplace transform is made of each term to predict the time response. All of these are simple exponential or sinusoidal time functions.

$$C_1 = \frac{R_0'}{R_0}\frac{1}{2\pi 10^9}g_1 \tag{2.9}$$

$$L_1 = \frac{R_0}{R_0'}\frac{1}{2\pi 10^9}g_2 \tag{2.10}$$

In addition to the tabulated data of low pass prototype filter elements, the values for these elements may be computed via execution of the equations found in [3].

A lowpass filter may be converted to a bandpass filter by employing a suitable mapping function. A mapping function is simply a mathematical change of variables such that a transfer function may be shifted in frequency. The mapping function may be intuitively or mathematically derived. A known low pass to bandpass mapping function may be illustrated mathematically as

$$f' = \frac{1}{FBW}\left(\frac{f}{f_0} - \frac{f_0}{f}\right) \tag{2.11}$$

$$FBW = \frac{\Delta f}{f_0} \tag{2.12}$$

where $f_0 = \sqrt{f_1 f_2}$ and $\Delta f = f_2 - f_1$ f_0, f_1 and f_2 represent the center, lower cutoff and higher cutoff frequencies of the corresponding bandpass filter response, respectively.

The schematic diagram of the bandpass filter, which was derived from the low pass prototype filter via the introduction of complementary elements and producing shunt and series resonators, is shown in Figure 2.3 This is a basic low pass to bandpass transformation, and unfortunately sometimes leads to component values, which are not readily available or have excessive loss.

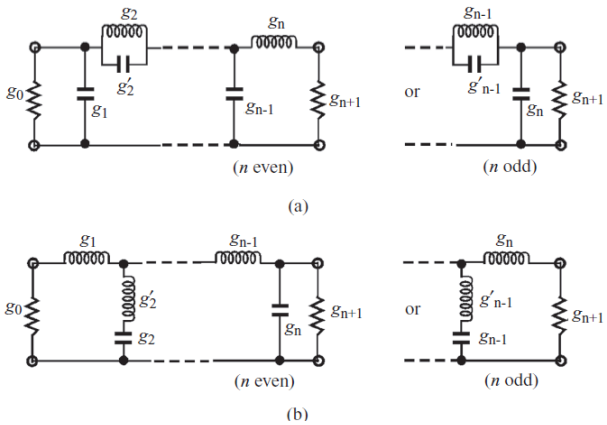

Figure 2.3: Chebyshev bandpass filter schematic.

2.2 Generalised Chebyshev Response

Modern filter synthesis allows the placement of transmission zeroes by the designer. Filters may be designed with asymmetrical responses to most efficiently attenuate low side or high side signals. Symmetrical responses are used where both lower and upper attenuations are important. This design is also useful where there are specific single frequencies to remove.

A filtering function with all transmission zeros,TZs, at infinity is called an all-pole function, and the most classical ones are the Butterworth and the Chebyshev filtering functions, seen above. On the other hand, introducing some TZs at finite frequencies, which tends to increase the selectivity of the amplitude response, generates different filtering functions, like the Generalized Chebyshev. The comparison between Chebyshev order four and Generalized Chebyshev order four with two TZs response is observed in Figure 2.4.

During the next chapters will be explained in more detail this response, its characteristics polynomials and how to implement it in a coupled circuit.

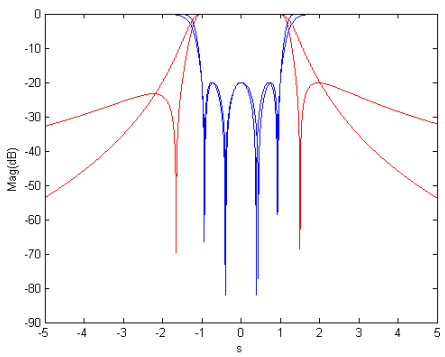

Figure 2.4: Comparison between order four Chebyshev response and order four with 2Tz generalized Chebyshev response (transmission in red and reflection in blue).

2.3 Filter of design

WF-00004 PCS Fullband Rx Filter from Lorch is taken as a reference in this project. We will try to design this filter with the methods explained along this project taking from a starting point this filter specifications.

Lorch Microwave's Wireless Products consist of transmit filters, receive filters, duplexers, harmonic suppression filters and integrated assemblies designed to exacting specifications and primarily used in infrastructure environments. Catalog standards and off the shelf availability provide cost effective solutions to the telecom industry. These units incorporate standard air dielectric designs and custom high Q ceramic

dielectric designs. In addition to the catalog standards, custom designs and generated to support specific customer requirements.

Cavity filters, explained in Chapter 5, are capable of high selectivity even under power loads of at least a megawatt. In the microwave range, cavity filters become more practical in terms of size and a significantly higher quality factor than lumped element filters. They are widely used for satellite and base station applications.

Lorch Microwave's cavity filter designs are available in the frequency range of 30 MHz to 40 GHz and with bandwidth options from less than 0.5% to over 66%. Cavity filters offer the user very low insertion loss, steep skirt selectivity, and narrower bandwidths than discrete component filters. Cavity filter performance is based on parts selection and physical layout of the helical coils, resonators, as well as the shape and size of the cavity housing.

Standard cavity filters generally are designed using aluminum as the base metal. As most raw metals are inherently lossy, filter housings are silver plated for improved electrical characteristics and current flow. Brass, copper, aluminum or bi-metal resonators are used to minimize frequency drift over temperature.

WF-00004 PCS FULLBAND RX FILTER

Lorch Microwave's WF-00004 PCS Fullband Rx Filter, shown in Figures 2.6 and 2.5, offers low insertion loss and high attenuation in the Tx band. This filter is compact in size and is well suited for many base station and laboratory applications. It is available with temperature compensation and weather proofing for use in more extreme conditions.

Figure 2.5: WF-00004 PCS Fullband Rx Filter.

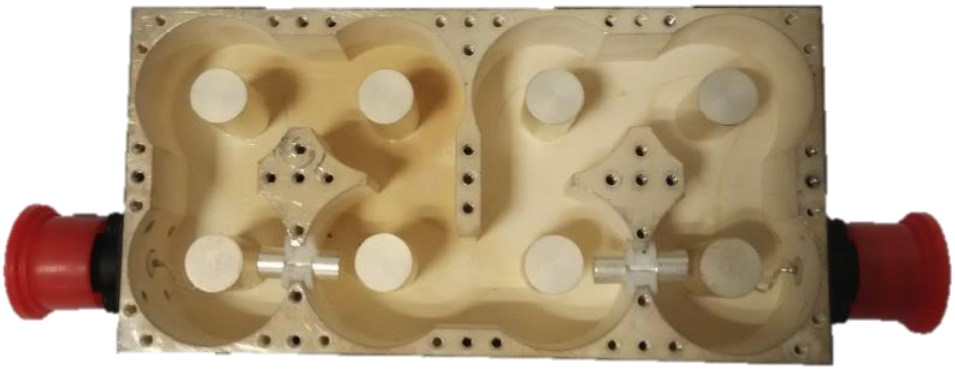

Figure 2.6: WF-00004 PCS Fullband Rx Filter without top cover.

WF-00004 ports have been connected to PNA-X network analyzer and we have been able to measure reflection and transmission parameters. From this measurements, shown in Figure 2.7, specifications are fixed, as shown above. Along this project the filter that is being designed is often compared with this and the persecuted response is based on the measurements shown.

The lowpass specifications for the filter of design will be:

- Generalized Chebyshev filtering function response.
- Order: N = 8.
- Return Loss: 20 dB.
- Transmission Zeros: [1.80866 1.82914 1.9285 1.9388] GHz, with equation 2.11 $\rightarrow$ [-2,327 -1,6542 1,5055 1,8237] rad/s.
- $f_1 = 1.84928\,GHz$ and $f_2 = 1.91225\,GHz$, with equation 2.12 $\rightarrow f_0 = 1.8805\,GHz$ and FBW=3.35%

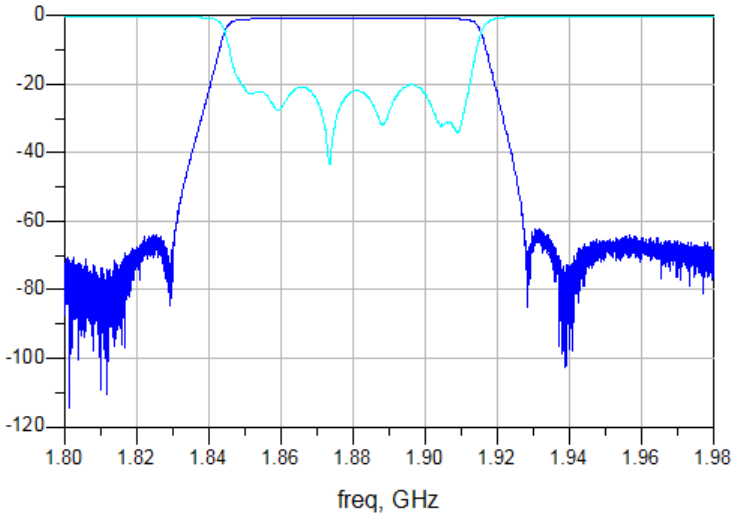

Figure 2.7: Filter measurement with PNA-X network analyzer shows transmission and reflection parameters.

Chapter 3

SYNTHESIS OF A GENERAL CLASS OF THE CHEBYSHEV FILTER FUNCTION

In this chapter, some important scattering parameter relations that are relevant for the synthesis of filter networks are reviewed. This is followed by a discussion of the general kind of Chebyshev function and its application in generating the transfer and reflection polynomials for equiripple filter characteristics with an arbitrary distribution of the transmission zeros.

3.1 Polynomial forms of the transfer and reflection parameters $S_{21}(s)$ and $S_{11}(s)$ for a two-port network

For the great majority of the filter circuits, it is initially considered two-port network; a “source port” and a “load port”, Figure 3.1.

For a two-port network, the scattering matrix is represented by a 2 x 2 matrix

$$\begin{bmatrix} b_1 \\ b_2 \end{bmatrix} = \begin{bmatrix} S_{11} & S_{12} \\ S_{21} & S_{22} \end{bmatrix} \begin{bmatrix} a_1 \\ a_2 \end{bmatrix} \tag{3.1}$$

where b_1 and b_2 are the power waves propagating away from ports 1 and 2, respectively, and $a_1$and a_2 are the power waves incident at ports 1 and 2, respectively.

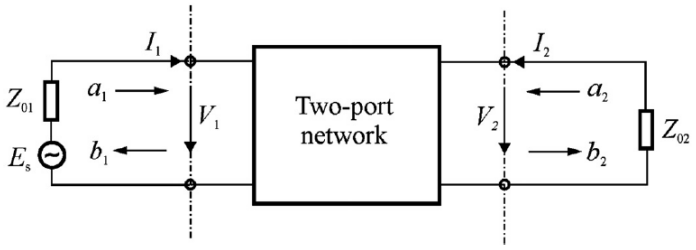

Figure 3.1: Two-port network.

If the network is pasive, lossless, and reciprocal, its 2 x 2 S-parameter matrix yields two conservation of energy equations

$$S_{11}(s)S_{11}(s)^* + S_{21}(s)S_{21}(s)^* = 1 \tag{3.2}$$

$$S_{22}(s)S_{22}(s)^* + S_{12}(s)S_{12}(s)^* = 1 \tag{3.3}$$

And one unique orthogonality equation

$$S_{11}(s)S_{12}(s)^* + S_{21}(s)S_{22}(s)^* = 0 \tag{3.4}$$

where the S parameters are now assumed to be functions of $s(= j\omega)$, the frequency variable.

As described in[4] in more detail; the input impedance of a terminated network is a positive real function, and its normalized impedance z can be expressed as

$$z(s) = \frac{n(s)}{d(s)} \tag{3.5}$$

where n(s) and d(s) represent the numerator and denominator polynomials and z(s) is a positive real function. Thus reflection coefficient p can be defined as

$$p(s) = \pm\frac{reflected\ wave}{incident\ wave} = \frac{z(s)-1}{z(s)+1} = \frac{n(s)-d(s)}{n(s)+d(s)} = \frac{F(s)}{E(s)} \tag{3.6}$$

The three polynomials are referred to as the characteristic polynomials. For lowpass prototype filter networks, their properties are summarized as follows:

1. F(s) is a polynomial with real coefficients, and its roots lie along the imaginary axis as conjugate pairs. F(s) can have multiple roots only at the origin. The roots represent frequencies at which no

power is reflected, often termed reflection zeros. At these frequencies, the filter loss is zero, and F(s) is a pure odd or even polynomial.

2. P(s) is a pure even polynomial with real coefficients. Its roots lie on the imaginary axis in conjugate pairs. Such roots represent frequencies at which no power is transmitted, and the filter loss is infinite. These frequencies are often referred to as transmission zeros,TZs, or attenuation poles.

3. E(s) is a strict Hurwitz polynomial, as all its roots lie in the left half of the s plane.

In the synthesis procedure, polynomials F(s) and P(s) are normalized so that their highest coefficients are unity. This is accomplished by extracting the highest coefficients of these polynomials and representing their ratio as a constant factor that can be readily absorbed within the ripple factor.

As described in[4] in more detail; the reflection parameter $S_{11}(s)$ at port 1 of the network is expressed as the ratio of two finite-degree polynomials E(s) and F(s), and real constant ε_R

$$S_{11}(s) = \frac{F(s)/\varepsilon_R}{E(s)} \tag{3.7}$$

where E(s) is an Nth-degree polynomial with complex coefficients $e_0, e_1, ...e_N$ where N is the degree of the filter network under consideration. Also F(s) is an Nth degree polynomial with complex coefficients $f_0, f_1, ...f_N$.

ε_R allows the normalization of the highest degree coefficients of E(s) and F(s) to unity (i.e., e_N and $f_N = 1$). Because this is a lossless passive network, E(s) is strictly Hurwitz; that is, all the roots of E(s) [poles of $S_{11}(s)$] are in the left half of the complex plane.

By reorganizing equation 3.2 and substituting for $S_{11}(s)$, it can be obtained

$$S_{21}(s)S_{21}(s)^* = 1 - \frac{F(s)F(s)^*/\varepsilon_R^2}{E(s)E(s)^*} = \frac{P(s)P(s)^*/\varepsilon}{E(s)E(s)^*}$$

Thus, the transfer parameter $S_{21}(s)$ can be expressed as the ratio of two polynomials

$$S_{21}(s) = \frac{P(s)/\varepsilon}{E(s)} \tag{3.8}$$

where: $P(s)P(s)^*/\varepsilon^2 = E(s)E(s)^* - F(s)F(s)^*/\varepsilon_R^2$

From equations 3.7 and 3.8 it is seen that $S_{11}(s)$ and $S_{21}(s)$ share a common denominator polynomial E(s). The numerator of $S_{21}(s)$, polynomial $P(s)/\varepsilon$, whose zeros are transmission zeros (TZs) of the filtering function. The degree $n_{fz}$of the polynomial P(s) corresponds to the number of finite-position TZs that the function transfer incorporates. This also implies that $n_{fz} < N$; otherwise, $S_{21}(s)$ exceeds unity as $s \to j\infty$, which is, of course, impossible for a passive network.

3.1.1 Realization of a TZ (transmission zero)

A transmission zero can be realized in two ways. The first case occurs when the degree n_{fz} is less than the degree N of the denominator polynomial E(s), and $s \to j\infty$. At $s \to \infty$, $S_{21}(s) = 0$ and this is known as transmission zero at infinity. When $0 < n_{fz} < N$, the number of TZ at infinity is N-n_{fz}.

The second case occurs when the frequency variable s coincides with an imaginary-axis root of its numerator polynomial P(s), that is $s = s_{0i}$where s_{0i} is a purely imaginary root of P(s). The zeros are not necessarily on the imaginary axis, and if there is one root s_{0i}, that is complex, there must be a second root $-s_{0i}^*$ to make up a pair having symmetry about the imaginary axis.

Consideration of the orthogonality unitary condition provides an important relation between the phases of the $S_{11}(s)$, $S_{22}(s)$, and $S_{21}(s)$ polynomials, and between the zeros of $S_{11}(s)$ and $S_{22}(s)$ in the complex plane. If we apply the reciprocity condition $S_{21}(s) = S_{12}(s)$ to the unitary conditions described in equations 3.2, 3.3 and 3.4 it is obtained

$$S_{11}(s)S_{11}(s)^* + S_{21}(s)S_{21}^* = 1 \tag{3.9}$$

$$S_{22}(s)S_{22}(s)^* + S_{21}(s)S_{21}^* = 1 \tag{3.10}$$

$$S_{11}(s)S_{21}(s)^* + S_{21}(s)S_{22}^* = 0 \tag{3.11}$$

These vector quantities are writen in polar coordinates and a series of equation rewritting is done with detail in[4] and the following important relationship is obtained:

$$-\theta_{n21}(s) + \frac{\theta_{n11}(s) + \theta_{n22}(s)}{2} = \frac{\pi}{2}(2k \pm 1) \tag{3.12}$$

Where $\theta_{n21}(s)$,... are the angles of the numerator polynomials of $S_{21}(s)$ etc.

This equation states that at any value of the frequency variable s, the difference between the angle of the $S_{21}(s)$ numerator vector, and the average of phases of the $S_{11}(s)$ and $S_{22}(s)$ numerator vectors must be an odd multiple of $\pi/2$ radians, that is, orthogonal. Some properties and rules are extracted from 3.12 in[4] and one is important for this project, specially for the later formation of polynomial P(s). Associated with the orthogonality condition; when the highest-degree coefficients of the Nth-degree polynomials E(s) and F(s), and the $n_{fz}(\leq N)$-degree polynomial P(s) are normalized to unity (monic polynomials), then the P(s) polynomial must be multiplied by j when the integer quantity $(N - n_{fz})$ is even. In other words, $(N - n_{fz})$ must be odd. When $N - n_{fz}$ is even, an extra $\frac{\pi}{2}$ rad must be added, adding $\frac{\pi}{2}$ to $\theta_{n21}(S)$ is equivalent of multiplying P(s) by j.

So, we can now calculate polynomial P(s) as a first step of design of the filter. The roots of the polynomial $P(s)$ are directly the transmission zeros, which we already know, and $(N - n_{fz})$ is even so it must be

multiplied by j, so $P(s) = (s+2.3271j)(s+1.6542j)(s-1.8238j)(s-1.5055j)$. We can easily know $P(s)$ coefficients using Matlab function *poly*, that output the polynomial of the given roots, and we obtain that $P(s) = js^4 + 6.6597js^2 - 10.57j$.

By applying the orthogonality condition to the scattering matrix, we obtain

For $(N-n_{fz})$ odd,

$$F(s)P(s)^* + P(s)F_{22}(s)^* = 0 \tag{3.13}$$

For $(N-n_{fz})$ even,

$$F(s)[jP(s)]^* + [jP(s)]F_{22}(s)^* = 0 \text{ or } F(s)P(s)^* - P(s)F_{22}(s)^* = 0 \tag{3.14}$$

For $(N-n_{fz})$ even or odd,

$$F(s)P(s)^* - (-1)^{(N-n_{fz})}P(s)F_{22}(s)^* = 0 \tag{3.15}$$

Where $F_{22}(s) = (-1)^N F(s)^*$

which is represented in te following S-matrix form:

$$\begin{bmatrix} S_{11} & S_{12} \\ S_{21} & S_{22} \end{bmatrix} = \frac{1}{E(s)} \begin{bmatrix} \frac{F(s)}{\varepsilon_R} & \frac{P(s)}{\varepsilon} \\ \frac{P(s)}{\varepsilon} & \frac{(-1)^{(n_{fz}+1)}F(s)^*}{\varepsilon_R} \end{bmatrix} \tag{3.16}$$

In a similar way, it can be obtained alternative forms to represent the S matrix by manipulating equation 3.15. Whatever the form, the unitary conditions will be satisfied.

From unitary conditions, two additional relationships are derived and later explained:

- The relationship between the real constants ε and ε_R used to normalize the polynomials P(s) and F(s), respectively.
- The alternating pole-principle, which allows the accurate determination of either E(s), F(s), or P(s) while knowing the other two.

3.2 Relationship between ε and ε_R

The transfer and reflection functions $S_{21}(s)$ and $S_{11}(s)$ were defined earlier in terms of their rational polynomials in equations 3.8 and 3.7 respectively, where E(s) and F(s) are Nth degree, P(s) is a polynomial of degree n_{fz}, the number of finite-position transmission zeros, and ε and ε_R are real constants normalizing P(s) and F(s) such that $|S_{21}(s)|$and $|S_{11}(s)|$ are ≤ 1 at any value of s, the frequency variable. It is assumed

that the three polynomials have been normalized such that their highest-power coefficients are unity. Supplemental to this, for the cases where $N - n_{fz}$ is an integer, the polynomial P(s) is multiplied by j to satisfy the unitary condition as described above.

The real constant ε is determined by evaluating P(s)/E(s) at a convenient value of s, where $S_{21}(s)$ or $S_{11}(s)$ are known, for instance, at $s = \pm j$, where the equiripple return loss level for Chebyshev filter or the 3dB (half-power point) for Butterworth filters is known. This sets the maximum level for $|S_{21}(S)|$ at 1, and if $n_{fz} < N$, $|S_{21}(S)| = 0$ at infinite frequency $s = \pm j\infty$. When $|S_{21}(S)| = 0$, the conservation of energy condition dictates that

$$|S_{11}(j\infty)| = \frac{1}{\varepsilon_R}\left|\frac{F(j\infty)}{E(j\infty)}\right| = 1 \tag{3.17}$$

Because the highest-degree coefficients (e_N and f_N) of E(s) and F(s), respectively, are unity, it is easily seen that $\varepsilon_R = 1$. When $n_{fz} = N$,that is, where all N available transmission zeros are at finite positions in the complex plane and therefore P(s) is an Nth-degree polynomial (fully canonical function), then the attenuation at $s = \pm j\infty$ is finite and ε_R is derived from the conservation of energy condition equation by

$$S_{11}(j\infty)S_{11}(j\infty)^* + S_{21}(j\infty)S_{21}(j\infty)* = 1 \tag{3.18}$$

$$\frac{F(j\infty)F(j\infty)^*}{\varepsilon_R^2 E(j\infty)E(j\infty)^*} + \frac{P(j\infty)P(j\infty)^*}{\varepsilon^2 E(j\infty)E(j\infty)^*} = 1 \tag{3.19}$$

For the fully canonical case, E(s), F(s), and P(s) are all Nth-degree polynomials with the highest-power coefficients =1. Therefore, we obtain

$$\frac{1}{{\varepsilon_R}^2} + \frac{1}{\varepsilon^2} = 1 \text{ or } \varepsilon_R = \frac{\varepsilon}{\sqrt{\varepsilon^2 - 1}} \tag{3.20}$$

which is slightly greater than unity since ε has to be >1.

Also, it is evident that for the fully canonical case, the insertion loss at $s = \pm j\infty$ is

$$S_{21}(\pm\infty) = \frac{1}{\varepsilon} = 20log_{10}\varepsilon \text{ dB} \tag{3.21}$$

and the return loss is

$$S_{11}(\pm\infty) = \frac{1}{\varepsilon_R} = 20log_{10}\varepsilon_R \text{ dB} \tag{3.22}$$

Although the fully canonical characteristics are rarely used for the synthesis of bandpass filters, they are sometimes used for bandstop filters.

The calculation of ε_R and ε of the filter of study will be useful as example; It is known from 2.3 and

3.4 that N=8 and $n_{fz} = 4$, so from 3.17 and explanation above $\varepsilon_r = 1$. And evaluating P(s)/E(s) at a convenient value of s where $S_{21}(s)$ or $S_{11}(s)$ are known, $s = \pm j$, leaves:

$$\varepsilon = \frac{1}{\sqrt{10^{RL/10} - 1}} \left| \frac{P(\omega)}{F(\omega)/\varepsilon_r} \right|_{\omega=\pm 1} \tag{3.23}$$

And therefore with equation 3.23 and using value of RL=20dB from 2.3 and values of $P(\omega)$ and $F(\omega)$ from 3.4 $\longrightarrow \varepsilon = 93.2344$ for the filter of design.

3.3 Alternating pole method for determination of the denominator polynomial E(s)

For the polynomial synthesis method to be described later, transmission zeros are prescribed in the complex plane, which defines the $S_{21}(s)$ numerator polynomial P(s). Then the coefficients of the $S_{11}(s)$ numerator polynomial F(s) are found using an analytic or recursive method explained in 3.4. It then remains to find the $S_{11}(s)$ and $S_{21}(s)$ denominator polynomial E(s) to complete the design of the filtering function.

If two of the three polynomials are known, the third may be derived from the conservation of energy equation (3.9) as follows:

$$S_{11}(s)S_{11}(s)^* + S_{21}(s)S_{21}(s)^* = 1 \text{ or } \frac{F(s)F(s)^*}{\varepsilon_R^2} + \frac{P(s)P(s)^*}{\varepsilon^2} = E(s)E(s)^* \tag{3.24}$$

The left-hand side (LHS) of equation 3.24 is constructed using polynomial multiplications to find polynomial E(s)E(s)*, which must be a scalar quantity. This means that the 2N roots of E(s)E(s)*, must form a symmetric pattern about the imaginary axis in the complex plane, so that at any frequency s product E(s)E(s)* is scalar.

Since it is known that the roots of E(s) are strictly urwitz, thse roots of E(s)E(s)* that are in the left-half plane must belong to E(s) and those in the right-half plane, to E(s)*. By choosing the N roots in the left-half plane, the polynomial E(s) is formed.

Although this method is completely general, it does mean working with double-degree polynomials, and sometimes, with higher degree filter functions, the roots of E(s)E(s)* tend to cluster around $s = \pm j$, leading to inaccurate root finding. An alternative method due to Rhodes and Alseyab[5] is presented here, with which the roots of E(s) can be found without having to determine the roots of polynomials of degree 2N.

By expanding equation in two different ways, we obtain

$$\varepsilon^2\varepsilon_R^2 E(s)E(s)^* = [\varepsilon_R P(s) + E(s)][\varepsilon_R P(s)^* + \varepsilon F(s)^*] - \varepsilon\varepsilon_R[P(s)^*F(s) + P(s)F(s)^* \tag{3.25}$$

and

$$\varepsilon^2\varepsilon_R^2 E(s)E(s)^* = [\varepsilon_R(jP(s)) + \varepsilon F(s)][\varepsilon_R(jP(s))^* + \varepsilon F(s)^*] - \varepsilon\varepsilon_R[(jP(s))^* F(s) + (jP(s))F(s)^* \quad (3.26)$$

Equation 3.25 is in the correct form for the cases where the integer quantity (N-n_{fz}) is odd. For the term on the extreme right to equal zero

$$P(s)^* F(s) = -P(s)F(s)^* \quad (3.27)$$

If the orthogonality unitary condition for (N-n_{fz}) odd [equation 3.13] is recalled, namely

$$F(s)P(s)^* + P(s)F_{22}(s)^* = 0 \quad (3.28)$$

it is obvious that equation 3.27 is valid only if $F(s) = F_{22}(s)$. This can happen only when all the zeros of F(s) lie on the imaginary axis and are coincident with those of $F_{22}(s)$.

Equation 3.26 is in the correct form for the cases where (N-n_{fz}) is even, where the polynomial P(s) must be multiplied by j. For the term on the extreme right to equal zero, the following condition must hold:

$$P(s)^* F(s) = P(s)F(s)^* \quad (3.29)$$

By recalling the orthogonality unitary condition, described in equation 3.14 for (N-n_{fz}) even, one have

$$F(s)P(s)^* - P(s)F_{22}(s)^* = 0 \quad (3.30)$$

and once more it can be seen that equation 3.29 can be satisfied only if $F(s) = F_{22}(s)$. Again, this can happen only when all the zeros of F(s) lie on the imaginary axis and are coincident with those of $F_{22}(s)$.

If the zeros of F(s) and $F_{22}(s)$ fulfill this condition, equations 3.25 and 3.26 for (N-n_{fz}) odd are reduced to

$$\varepsilon^2\varepsilon_R^2 E(s)E(s)^* = [\varepsilon_R P(s) + \varepsilon F(s)][\varepsilon_R P(s)^* + \varepsilon F(s)^*] = [\varepsilon_R P(s) + \varepsilon F(s)][\varepsilon_R P(s) + \varepsilon F(s)]^* \quad (3.31)$$

and for (N-n_{fz}) even

$$\varepsilon^2\varepsilon_R^2 E(s)E(s)^* = [\varepsilon_R(jP(Ss)) + \varepsilon F(s)][\varepsilon_R(jP(s))^* + \varepsilon F(Ss)] = [\varepsilon_R(jP(s)) + \varepsilon F(s)][\varepsilon_R(jP(s)) + \varepsilon F(s)]^* \quad (3.32)$$

In the ω plane, P(ω) and F(ω) will ave purely real coefficients. Use 3.32 modified as follows to find the ω-plane singularities for (N-n_{fz}) even or odd:

$$\varepsilon^2\varepsilon_R^2 E(\omega)E(\omega)^* = [\varepsilon_R P(\omega) - j\varepsilon F(\omega)][\varepsilon_R P(\omega) - j\varepsilon F(\omega)]^* \tag{3.33}$$

Rooting one of the two terms on the right-hand side (RHS) of equation 3.32 results in a pattern of singularities alternating between the left-half and right-half planes, as depicted in Figure 3.2.

Rooting the other term will give the complementary set of singularities, completing the symmetry of the pattern about the imaginary axis and ensuring that the RHS of 3.32 is properly scalar as the LHS demands.

As a result, it is necessary to form only one of the two terms in equation 3.32 from the known P(s) and F(s) polynomials, and then root the resultant Nth-degree polynomial with complex coefficients to obtain the singularities. Knowing that the polynomial E(s) must be Hurwitz, any singularity in the right half-plane (RHP) plane can be reflected about the imaginary axis to lie in the image position in the left half-plane (LHP) plane. Now, knowing the positions of the N singularities in the LHP, we can form the polynomial E(s). In finding E(s), we only have to deal with Nth-degree polynomials; also because the alternating singularities tend to be less clustered about $s = \pm j$, greater accuracy is guaranteed.

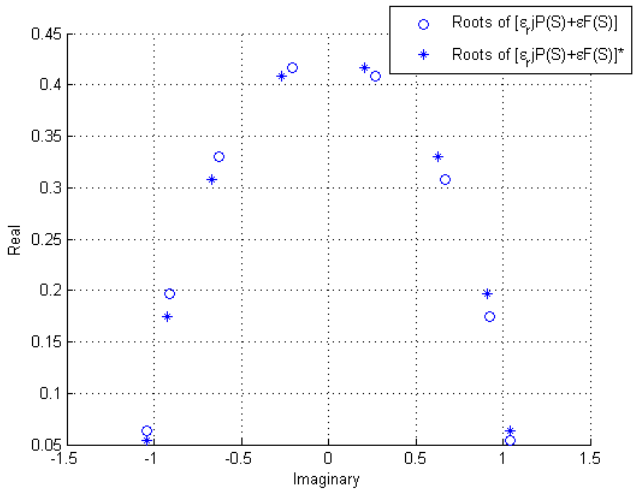

Figure 3.2: Obtained singularities of polynomials for the filter of study, (N-n_{fz}) even.

This procedure explained in this section can be implemented in a Matlab code like the one shown in APPENDIX A.

And obtain with it the $E(s)$ polynomial coefficients and roots of the filter of study:

Coefficients

$E(s) = s^8 + s^7(1.951 - 0.1164j) + s^6(3.996 - 0.2306j) + s^5(4.637 - 0.4407j) + s^4(4.645 - 0.4889j) +$

$s^3(3.243-0.4407j)+s^2(1.735-0.2693j)+s(0.6035-0.1131j)+(0.1113-0.02436j)$

Roots

$E(s)=(s+(1.044j+0.06298))(s+(0.6279j+0.3303))(s+(0.205j+0.4172))(s+(0.912j+0.1964))(s+(0.1744-0.9261j))(s+(0.3077-0.6713j))(s+(0.4079-0.2694j))(s+(0.05423-1.039j))$

3.4 Recursive Technique

Since, by definition, a Chebyshev function has all its reflection zeros on the real axis of the ω plane, the alternating pole formula for a lossless network, as described by equation 3.33, is as follows:

$$S_{21}(\omega)S_{21}(\omega)^* = \frac{P(\omega)P(\omega)^*}{\varepsilon^2 E(\omega)E(\omega)^*} = \frac{1}{\left[1-j\frac{\varepsilon}{\varepsilon_R}kC_N(\omega)\right]\left[1-j\frac{\varepsilon}{\varepsilon_R}kC_N(\omega)^*\right]} \tag{3.34}$$

where $kC_N(\omega)=\frac{F(\omega)}{P(\omega)}$ and k is a constant.

$C_N(\omega)$ is known as the filter function of degree N, and its poles and zeros are the roots of $P(\omega)$ and $F(\omega)$, respectively. For the general Chebyshev characteristic, it has de form[6]

$$C_N(\omega) = cosh\left[\sum_{n=1}^{N} cosh^{-1}(x_n(\omega))\right] \tag{3.35}$$

or, by using the identity $cosh\theta = cos\,j\theta$, the alternative expression for $C_N(\omega)$ is given by

$$C_N(\omega) = cos\left[\sum_{n=1}^{N} cos^{-1}(x_n(\omega))\right] \tag{3.36}$$

where $x_n(\omega)$ is a function of the frequency variable ω. For analyzing $C_N(\omega)$, equation 3.35 can be adopted for $|\omega|\geq 1$ and equation 3.36, for $|\omega|\leq 1$.

To properly represent a Chebyshev function,

$$x_n(\omega) = \frac{\omega - 1/\omega_n}{1-\omega/\omega_n} \tag{3.37}$$

Where ω_n is the position of the nth transmission zero.

From equation 3.35 and some operations explained in detail in[4] equation 3.35 becomes

$$C_N(\omega) = \frac{1}{2}\left[\frac{\prod_{n=1}^{N}\left[(\omega-1/\omega_n)+\sqrt{(1-1/\omega_n^2)}\omega\right]+\prod_{n=1}^{N}\left[(\omega-1/\omega_n)-\sqrt{(1-1/\omega_n^2)}\omega\right]}{\prod_{n=1}^{N}\left[1-\omega/\omega_n\right]}\right] = \tag{3.38}$$

$$= \frac{1}{2}\left[\frac{\prod_{n=1}^{N}(C_n + d_n) + \prod_{n=1}^{N}(C_n - d_n)}{\prod_{n=1}^{N}[1 - \omega/\omega_n]}\right]$$

where

$$c_n = (\omega - \frac{1}{\omega_n}) \text{ and } d_n = \omega' \sqrt{1 - \frac{1}{\omega_n^2}}$$

In comparison with equation 3.34, it is obvious that the denominator of $C_N(\omega)$ has the same zeros as $P(\omega)$ the numerator polynomial of $S_{21}(\omega)$ generated from the prescribed transmission zeros ω_n. From equation 3.34 it is also observed that the numerator of $C_N(\omega)$ has the same zeros as the numerator $F(\omega)$ of $S_{11}(\omega)$, and appears at first to be a mixture of two finite-degree polynomials, one in the variable ω purely, whilst the other has each coefficient multiplied by the transformed variable ω'.

However, the coefficients multiplied by ω'cancel each other when equation 3.38 is multiplied out. This is best proven by demonstration, by multiplying out left- and right-hand product terms in the numerator of $C_N(\omega)$ in 3.38 for a few low values of N:

For N=1, Num$[C_1(\omega)]$=$\frac{1}{2}\left[\prod_{n=1}^{1}(c_n + d_n) + \prod_{n=1}^{1}(c_n - d_n)\right] = c_1$.

For N=2, Num$[C_2(\omega)]$=$c_1c_2 + d_1d_2$.

For N=3, Num$[C_3(\omega)]$=$(c_1c_2 + d_1d_2)c_3 + (c_2d_1 + c_1d_2)d_3$.

(and so on).

At each stage, the expansions result in a sum of factors, where each factor is composed of multiples of c_n and $d_n$elements. Because of the positive sign in the LH product term in equation 3.38, the c_n, d_n factors, resulting from multiplying out the LH term, are always positive in sign. Multiplying out the RH product term in equation 3.38 produces the same c_n, d_n factors; however, the negative sign indicates that those factors containing an odd number of d_n elements are negative in sign and are canceled with the corresponding factors from the LH product term.

Now, the remaining factors contain only the even numbers of d_n elements. Consequently, $\omega' = \sqrt{\omega^2 - 1}$, which is a common multiplier for all the d_n elements [equation 3.38], is raised by even powers only, producing subpolynomials in the variable ω. As a result, the numerator of $C_N(\omega)$ will be a polynomial in the variable ω only.

These relationships can be used to develop a simple algorithm to determinate the coefficients of the numerator polynomial of $C_N(\omega)$. Normalizing Num$[C_N(\omega)]$ to set its highest-degree coefficient to unity yields $F(\omega)$, the numerator of $S_{11}(\omega)$.

The numerator of equation 3.38 may be written as

$$Num[C_N(\omega)] = \frac{1}{2}\left[G_N(\omega) + G'_N(\omega)\right] \tag{3.39}$$

where

$$G_n(\omega) = \prod_{n=1}^{N}(c_n + d_n) = \prod_{n=1}^{N}\left[(\omega - \frac{1}{\omega_n}) + \omega'\sqrt{(1 - \frac{1}{\omega_n^2})}\right] \tag{3.40}$$

and

$$G'_n(\omega) = \prod_{n=1}^{N}(c_n - d_n) = \prod_{n=1}^{N}\left[(\omega - \frac{1}{\omega_n}) - \omega'\sqrt{(1 - \frac{1}{\omega_n^2})}\right] \tag{3.41}$$

The method for computing the coefficients of Num$[C_N(\omega)]$ is a recursive technique, where the solution for the nth degree is built up from the results of the (n-1)th degree. First, it is considered the polynomial $G_N(\omega)$ [equation 3.41]. This polynomial can be rearranged into two polynomials; $U_N(\omega)$ and $V_N(\omega)$, where the $U_N(\omega)$ polynomial contains the coefficients of the terms in the variable ω only, whereas each coefficient of the auxiliary polynomial $V_N(\omega)$ is multiplied by the transformed variable ω'

$$G_N(\omega) = U_N(\omega) + V_N(\omega) \tag{3.42}$$

where

$$U_N(\omega) = u_0 + u_1\omega + u_2\omega^2 + ... + u_N\omega^N \tag{3.43}$$

and

$$V_N(\omega) = \omega'(v_0 + v_1\omega + v_2\omega^2 + ... + v_N\omega^N \tag{3.44}$$

The recursion cycle is initiated with the terms corresponding to the first prescribed transmission zero ω_1, that is, by setting N=1 in equations 3.40 and 3.42:

$$G_1 = [c_1 + d_1] = (\omega - 1/\omega_1) + \omega'\sqrt{1 - \frac{1}{\omega_1^2}} = U_1(\omega) + V_1(\omega) \rightarrow \begin{cases} U_1(\omega) = (\omega - 1/\omega_1) \\ V_1(\omega) = \omega'\sqrt{1 - 1/\omega_1^2} \end{cases} \tag{3.45}$$

For the first cycle of the process, $G_1(\omega)$ has to be multiplied by the terms corresponding to the second prescribed zero ω_2 [equation 3.40], given by

$$G_2(\omega) = G_1(\omega)[c_2 + d_2] = [U_1(\omega) + V_1(\omega)]\left[(\omega - \frac{1}{\omega_2}) - \omega'\sqrt{(1 - \frac{1}{\omega_2})}\right] = U_2(\omega) + V_2(\omega) \tag{3.46}$$

Lets multiply out this expression for $G_2(\omega)$, and again allocating terms purely in ω to $U_2(\omega)$, terms multiplied by ω' to $V_2(\omega)$, and recognizing that $\omega' V_n(\omega)$ results in $(\omega^2-1)(v_0+v_1\omega+v_2\omega^2+...+v_n\omega^n)$ [equation 3.42] , a polynomial purely in ω and therefore to be allocated to $U_n(\omega)$:

$$\begin{cases} U_2(\omega) = \omega U_1(\omega) - \frac{U_1(\omega)}{\omega_2} + \omega' \sqrt{1-1/\omega_2^2} V_1(\omega) \\ V_2(\omega) = \omega V_1(\omega) - \frac{V_1(\omega)}{\omega_2} + \omega' \sqrt{1-1/\omega_2^2} U_1(\omega) \end{cases} \tag{3.47}$$

Having obtained these new polynomials $U_2(\omega)$ and $V_2(\omega)$, the cycle is repeated with the third prescribed zero, and so on until all N of the prescribed zeros (including those at $\omega_n = \infty$) are used, specifically, (N-1) cycles.

This procedure may be programmed in Matlab as shown in the code given below.

```
1
2  function [ Roots, Coeffs ] = F(zero)
3
4  syms w w2
5
6  N=length(zero); %number of transmission zeros to implement, included
       those at infinity
7
8  for n=1:N
9       if n==1 %initialize with first prescribed zero w1 (1)
10      U(1)=w-(1/zero(1));
11      V(1)=sqrt(w^2-1)*sqrt(1-1/(zero(1)^2));
12       elseif zero(n)==0 %multiply zeros that are at infinity (3)
13      U(n)=w*U(n-1)+sqrt(w^2-1)*V(n-1);
14      V(n)=w*V(n-1)+sqrt(w^2-1)*U(n-1);
15       else %multiply in second and subsequent prescribed zeros (2)
16      U(n)=w*U(n-1)-U(n-1)/(zero(n))+sqrt(w^2-1)*sqrt(1-1/(zero(n)^2))*
       V(n-1); %
17       V(n)=w*V(n-1)-V(n-1)/(zero(n))+sqrt(w^2-1)*sqrt(1-1/(zero(n)^2))*
       U(n-1);
18       end
19 end
20
21 Coeffs=sym2poly(U(N)) %polynomial U_N(w)
22 Roots=roots(Coeffs) %polynomial F(w) roots
23
24 end
```

If the same process is repeated for $G'_N(\omega) = U`_N(\omega) + V'(\omega)$ [equation 3.41], then $U'_N(\omega) = U_N(\omega)$ and $V'_N(\omega) = -V_N(\omega)$. Therefore, from equations 3.39 and 3.42, it is obtained

$$Num[C_N(\omega)] = \frac{1}{2}[G_N(\omega) + G'_N(\omega) = \frac{1}{2}((U_N(\omega) + U'_N(\omega)) + ((V_N(\omega) + V'_N(\omega)) = U_N(\omega) \qquad (3.48)$$

Equation 3.48 demonstrates that the numerator of $C_N(\omega)$ [which has the same zeros $F(\omega)$] is equal to $U_N(\omega)$ after (N-1) cycles of this recursion method. Now the zeros of F(ω) are revealed by finding roots of $U_N(\omega)$, and along with the prescribed zero polynomial $P(\omega)/\varepsilon$, the denominator polynomial $E(\omega)$ can be constructed.

In the case of the filter of study, there are 4 zeros to implement, section2.3, $\omega_5, \omega_6, \omega_7$ and ω_8 are taken at infinity, and applying the Matlab function it is obtained:

Coefficients

$F(\omega) = \omega^8 - 0.1164\omega^7 - 2.093\omega^6 + 0.2123\omega^5 + 1.392\omega^4 - 0.1129\omega^3 - 0.3054\omega^2 + 0.01559\omega + 0.01114$

$F(s) = s^8 + 2.093s^6 + 1.392s^4 + 0.3054s^2 + 0.01114$

Roots

$F(\omega) = (\omega + 0.5725)(\omega + 0.1852)(\omega + 0.8471)(\omega + 0.9832)(\omega - 0.9854)(\omega - 0.2415)(\omega - 0.8648)(\omega - 0.6127)$

$F(s) = (s + 0.5725j)(s + 0.1852j)(s + 0.8471j)(s + 0.9832j)(s - 0.9854j)(s - 0.2415j)(s - 0.8648j)(s - 0.6127j)$

Due to the order is N=8 the maximum number of transmission zeros positioned in finite frequencies is 4. For the polynomial synthesis methods described, the number of transmission zeros with finite positions in the s plane n_{fz} must be $\leq N$. If $n_{fz} \leq N$, those zeros without finite positions must be placed at infinity. Although the N+2 coupling matrix (Chapter 4) can accommodate fully canonical filtering functions (i.e. $n_{fz} = N$), the N x N matrix can accommodate a maximum of only N-2 finite-position zeros (minimum path rule[a]). In synthesizing the polynomials for the N x N coupling matrix, at least two of the transmission zeros must be placed at infinity.

Finally, in order to check if calculated polynomials are correct, Lowpass transmission and reflection responses, determined by means of the evaluation of equations 3.7 and 3.8, are plotted in Figure 3.3. The filter satisfy the required specifications of transmission zeros and return loss, so it's similar to measurements.

[a]The minimum path rule is a simple formula for calculating the number of finite-position transmission zeros (i.e., those that are not at $\omega = \pm\infty$) that an Nth-degree direct-coupled resonator network can realize. If the number of resonators in the shortest path (along nonzero interresonator couplings) between the input (source) and the output (load) terminals of a network equals n_{min}, ten the maximum number of finite-position TZs (n_{fz}) tat the network may realize is $n_{fz} = N - n_{min}$.

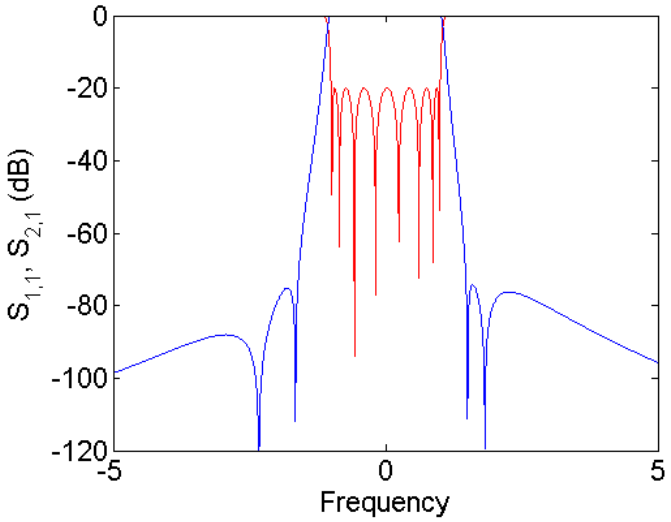

Figure 3.3: Transmission and reflection parameters of the filter obtained with the polynomials calculated previously.

Chapter 4

COUPLING MATRIX SYNTHESIS OF FILTER NETWORKS

4.1 Synthesis of network-circuit approach

In the previous chapters, methods were established to derive the transfer and reflection polynomials for lowpass prototype filter functions. The next step in the design process is to translate these polynomials into a electrical circuit prototype from which a real microwave filter may be developed. Two methods for doing this are available: the classical circuit synthesis method and the direct coupling matrix synthesis approach. Due to the aims of this project we will focus in network analysis but in this section, the circuit synthesis approach, based on the [ABCD] transfer matrix, or the "chain" matrix, as it is sometimes known, is briefly introduced only to introduce some formulas that will be later used.

For a two-port network operating between unity source and load terminations, the [ABCD] matrix representing the network has the following form[7]

$$[ABCD] = \frac{1}{P(s)/\varepsilon} \begin{bmatrix} A(s) & B(s) \\ C(s) & D(s) \end{bmatrix} \tag{4.1}$$

where

$$S_{12}(s) = S_{21}(s) = \frac{P(s)/\varepsilon}{E(s)} = \frac{2P(s)/\varepsilon}{A(s)+B(s)+C(s)+D(s)} \tag{4.2}$$

$$S_{11}(s) = \frac{F(s)/\varepsilon_R}{E(s)} = \frac{A(s)+B(s)-C(s)-D(s)}{A(s)+B(s)+C(s)+D(s)} \tag{4.3}$$

$$S_{22}(s) = \frac{(-1)^N F(s)^*/\varepsilon_R}{E(s)} = \frac{D(s)+B(s)-C(s)-A(s)}{A(s)+B(s)+C(s)+D(s)} \tag{4.4}$$

The j that multiplies P(s) in the denominator of equation 4.1 allows the crosscouplings to be extracted as inverters, and is there, in addition to the j that multiplies P(s) when N-n_{fz} is even, to preserve the orthogonality unitary condition (see section 3.3).

From equation 4.1, it is immediately clear that the A(s), B(s), C(s), and D(s) polynomials share a common denominator polynomial P(s)/ε. It is demonstrated that these polynomials can be built up from the elements of the circuit that models the real microwave filter, and then related to the coefficients of the E(s) and F(s)/ε_R polynomials, which, together with P(s)/ε, represent the desired transfer and reflection performance of the filter, respectively.

A coupled-cavity microwave bandpass filter is realized directly from lowpass prototype circuits of the type shown in Figure 2.1. After the addition of the series and parallel resonating components [to form the bandpass prototype (BPP)], and the appropriate scaling to the center frequency and bandwidth of the RF bandpass filter, the design of the microwave structures or devices used to realize the elements of the bandpass circuit becomes apparent. These resonators are realized in the microwave structure by elements such as coaxial resonators. Figure 4.1 illustrates the procedure for a fourth-degree all-pole filter after having obtained the transfer and reflection polynomials seen in equations 4.2 ,4.3 and 4.4 that will set the basis of the circuit synthesis.

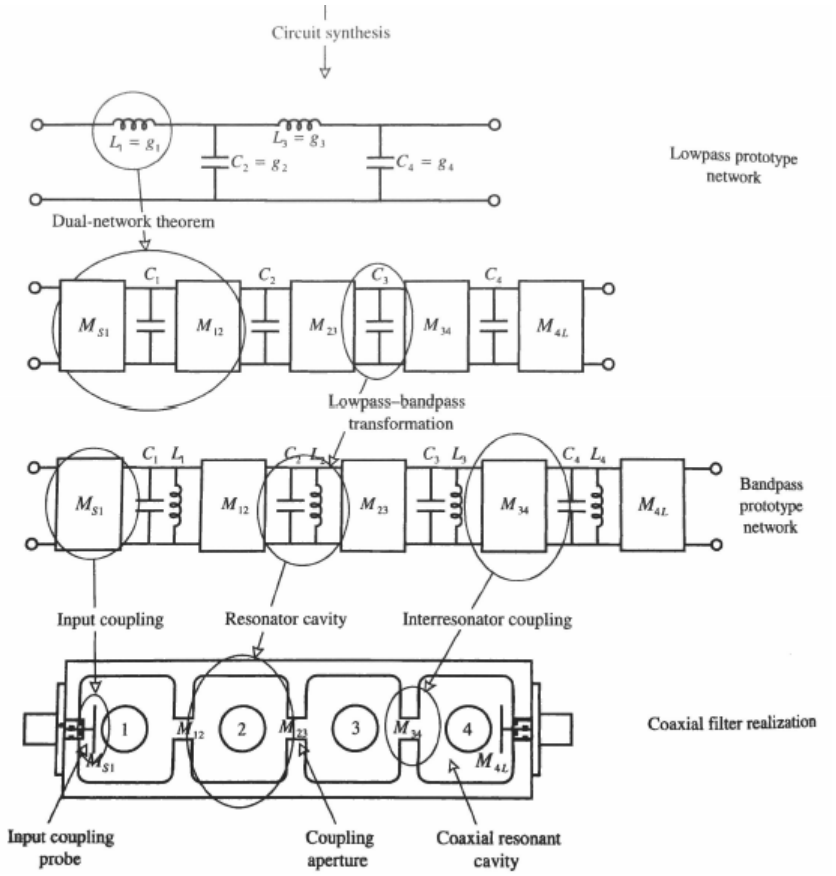

Figure 4.1: Steps in the synthesis process for a fourth-order coaxial resonator bandpass filter.

The synthesis of the [ABCD] polynomials for circuits with inverters is deeply explained in[4], broadly outlined that is obtained by multiplying [ABCD] matrices of cascaded elements as capacitors and inverters. These cascade operations reveal some important features of the A(s), B(s), C(s), and D(s) polynomials that represent the filter ladder network. All are polynomials in variable s with real coefficients and are even or odd, depending on whether N is even or odd. Idependently of whether N is even or odd, B(s) is of degree N and is the highest degree. A(s) and D(s) are of degree N-1, and C(s) is the lowest degree N-2.

Next, we relate the A(s), B(s), C(s), and D(s) polynomials with the $S_{21}(s)$ and $S_{11}(s)$ transfer and reflection polynomials (E(s), P(s)/ε and F(s)/ε_R). For the general case, the coefficients of E(s) and F(s) can have complex coefficients. To account for the general cases it is necessary to add a frequency-independent reactance (FIR) in parallel with each shunt frequency-dependent element (the capacitors C_i) such that the value of the admittance at each node, instead of being simply sC_i, now becomes $sC_i + jB_i$.

The effect of adding the FIRs at each node is to conver the A(s), B(s), C(s) and D(s) polynomials for the ladder network into complex-even and complex-odd forms, that is, their coefficients alternate between purely real and purely imaginary as the power of s increases.

Knowing now the form of the A(s), B(s), C(s), and D(s) polynomials, of the polynomials constituting $S_{11}(s)$ and $S_{21}(s)$ (E(s), P(s)/ε and F(s)/ε_R), and also the relationship between them [equation 4.1], A(s), B(s), C(s), and D(s) may be directly expressed in terms of the coefficients of E(s) and F(s)/ε_R :

N even:

$$\begin{aligned} A(s) &= Im(e_0+f_0)+jRe(e_1+f_1)s+Im(e_2+f_2)s^2+...+jIm(e_N+f_N)s^N \\ B(s) &= jRe(e_0+f_0)+Im(e_1+f_1)s+jRe(e_2+f_2)s^2+...+Re(e_N+f_N)s^N \\ C(s) &= jRe(e_0-f_0)+Im(e_1-f_1)s+jRe(e_2-f_2)s^2+...+Re(e_N-f_N)s^N \\ D(s) &= Im(e_0-f_0)+jRe(e_1-f_1)s+Im(e_2-f_2)s^2+...+jIm(e_N-f_N)s^N \end{aligned} \tag{4.5}$$

N odd

$$\begin{aligned} A(s) &= Re(e_0+f_0)+jIm(e_1+f_1)s+Re(e_2+f_2)s^2+...+jIm(e_N+f_N)s^N \\ B(s) &= jIm(e_0+f_0)+Re(e_1+f_1)s+jIm(e_2+f_2)s^2+...+Re(e_N+f_N)s^N \\ C(s) &= jIm(e_0-f_0)+Re(e_1-f_1)s+jIm(e_2-f_2)s^2+...+Re(e_N-f_N)s^N \\ D(s) &= Re(e_0-f_0)+jIm(e_1-f_1)s+Re(e_2-f_2)s^2+...+jIm(e_N-f_N)s^N \end{aligned} \tag{4.6}$$

Here, e_i and f_i, i=0,1,2,...,N, are complex coefficients of E(s) and F(s)/ε_R respectively.

It is easily demonstrated that these polynomials satisfy the equation set 4.1, and are the correct form for the representation of the electrical performance of a passive, reciprocal, lossless microwave circuit.

As described in next section, short-circuit admittance parameters (y parameters) are used for the direct synthesis of coupling matrices for filter networks. At this stage, the y-parameter matrix [y], later used in section 4.2, is found by using the [ABCD] as follows

$$\frac{1}{P(s)/\varepsilon}\begin{bmatrix} A(s) & B(s) \\ C(s) & D(s) \end{bmatrix} \Longrightarrow \begin{bmatrix} y_{11}(s) & y_{12}(s) \\ y_{21}(s) & y_{22}(s) \end{bmatrix} = \frac{1}{y_d(s)}\begin{bmatrix} y_{11n}(s) & y_{12n}(s) \\ y_{21n}(s) & y_{22n}(s) \end{bmatrix} = \frac{1}{B(s)}\begin{bmatrix} D(s) & -\Delta_{ABCD}\frac{P(s)}{\varepsilon} \\ \frac{P(s)}{\varepsilon} & A(s) \end{bmatrix} \tag{4.7}$$

where $y_{ijn}(s)$, i,j=1,2, are the numerator polynomials of $y_{ij}(s)$, $y_d(s)$ is their common denominator polynomial, and Δ_{ABCD} is the determinant of the [ABCD] matrix, which for a reciprocal network, Δ_{ABCD}=1 . From this, it becomes clear that

$$\begin{aligned} y_d(s) &= B(s) \\ y_{11n}(s) &= D(s) \\ y_{22n}(s) &= A(s) \\ y_{21n}(s) = Y_{12n}(s) &= -\frac{P(s)}{\varepsilon} \end{aligned} \tag{4.8}$$

The y(s) polynomials have the same form as the [ABCD] polynomials; namely, their coefficients alternate between purely real and purely imaginary as the power of s increases, $y_d(s)$ is of degree N, $y_{11n}(s)$

and $y_{22n}(s)$ are of degree N-1, and $y_{21n}(s)$ and $y_{12n}(s)$ are of degree n_{fz} (the number of finite-position transmission zeros). The short-circuit admittance parameters are used for the direct coupling matrix synthesis method described in the next section.

4.2 Coupling matrix

In this section, it is examined the coupling matrix representation of a microwave filter circuit. Modeling the circuit in matrix form is particularly useful because matrix operations can then be applied, such as inversion, similarity transformation, and partitioning. Such operations simplify the synthesis, reconfiguration of the topology, and performance simulation of complex circuits. Moreover, the coupling matrix is able to include some of the real-world properties of the elements of the filter. Each element in the matrix can be identified uniquely with an element in the finished microwave device. This enables us to account for the attributions of electrical characteristics of each element, such as Q_u, values for each resonator cavity, different dispersion characteristics for the various types of mainline coupling and cross-coupling within the filter. This is difficult or impossible to achieve with a polynomial representation of the filter's characteristics.

Atia and Williams introduced the concept of coupling matrix as applied to dual-mode symmetric waveguide filters[8]. The circuit model they investigated was a band-pass prototype, which has the form shown in Figure 4.2 . The circuit is comprised of a cascade of lumped-element series resonators inter-coupled by transformers. The circuit model only supports symmetric characteristics. Cameron introduced the concept of frequency-invariant reactance (FIR), enabling the circuit to represent asymmetric characteristics[9].

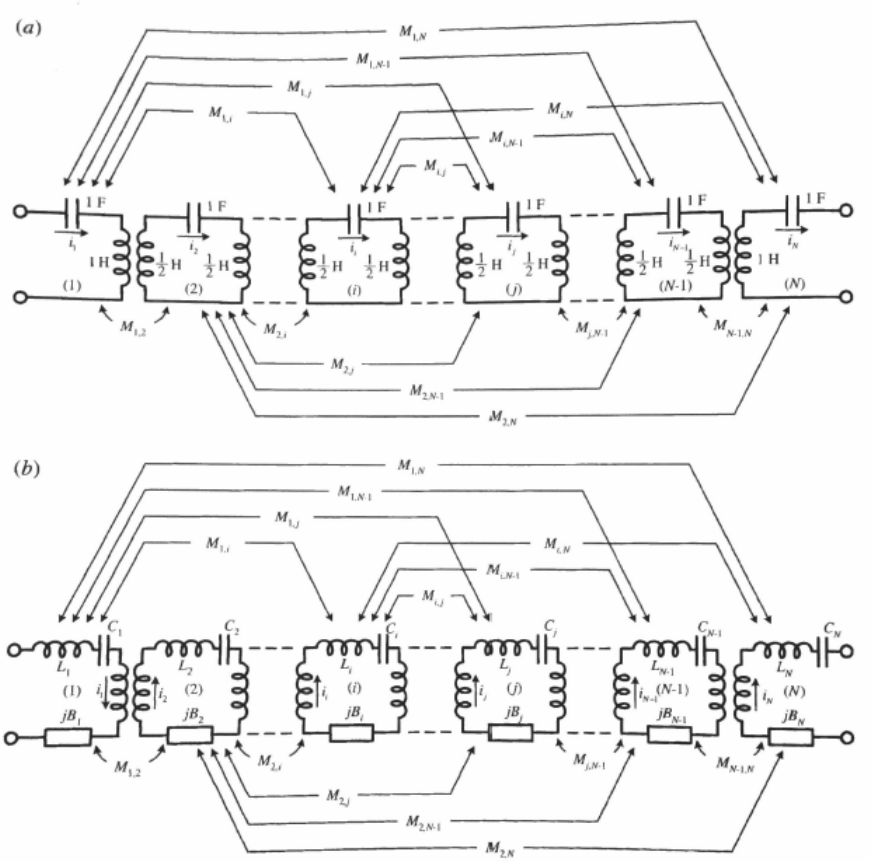

Figure 4.2: Multicoupled series-resonator bandpass prototype network: (a) classical representation; (b) modified to include FIR elements and separate self-inductors.

Because the coupling elements are frequency-invariant, the series resonator circuit itself can be transformed to the lowpass domain by the following steps:

1. Replace all the mutual inductive couplings, provided by transformers, with inverters with the same values as the mutual couplings of the transformers. The inverters then provides the same amount of coupling energy between the resonator nodes as the transformers, and with the same 90º phase change.

2. Transform the bandpass network to a lowpass prototype network with the band edges at $\omega = \pm 1$ by letting the value of the series capacitance go to infinity (zero series impedance).

In Figure 4.3 there is represented the low-pass prototype of a multicoupled asymmetric network with series resonators. This is the form of the circuits synthesized from the filter $S_{21}(s)$ and $S_{11}(s)$ polynomials. Because the coupling elements are assumed frequency-invariant, the synthesis in the low-pass or bandpass domains yields the same values for the circuit elements, and under analysis the insertion loss and

rejection amplitudes are the same. The frequency variables in the low-pass and band-pass domains are connected by the lumped-element frequency mapping formula

$$s = j\frac{\omega_0}{\omega_2 - \omega_1}\left[\frac{\omega_{BP}}{\omega_0} - \frac{\omega_0}{\omega_{BP}}\right] \tag{4.9}$$

where $\omega_0 = \sqrt{\omega_1 \omega_2}$ is the center frequency of the bandpass prototype, $\omega_2$and ω_1 are the upper and lower band-edge frequencies, respectively, and ω_{BP} is the bandpass frequency variable.

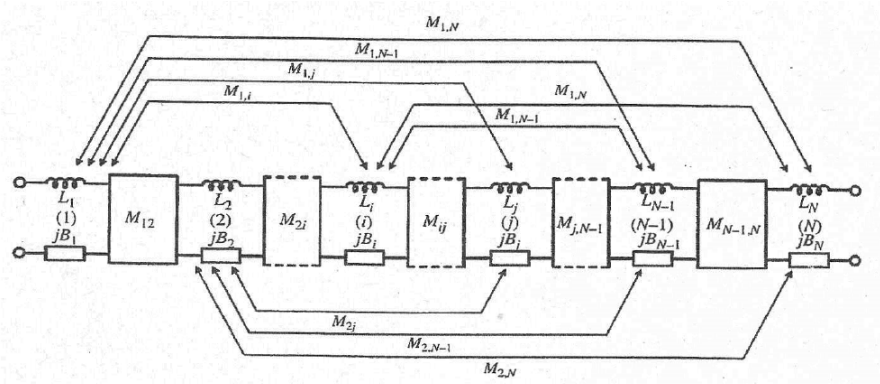

Figure 4.3: Multicoupled series-resonator low-pass NxN prototype network.

4.3 Formation of the general NxN coupling matrix and its Analysis

The two-port network of Figure 4.2 (in either its BPP or LPP form) operates between a voltage source generating $e_g$volts and an internal impedance of R_S (Ω) and a load impedance of R_L (Ω). As a series resonator circuit with currents circulating in the loops, the overall circuit including te source and load terminations are represented with the impedance matrix [z'] in Figure 4.4.

Kirchoff's nodal law (stating that the vector sum of all the currents entering a node is equal to zero) is applied to the currents circulating in te series resonators of the circuit shown in Figure 4.2a, leading to a series of equations that may be represented with the matrix equation[8]

$$[e_g] = [z'][i] \tag{4.10}$$

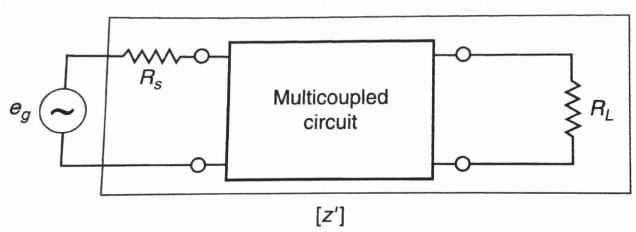

Figure 4.4: Overall impedance matrix [Z'] of the series resonator circuits of Figure 4.3 operating between a source impedance R_S and a load impedance R_L.

where [z'] is the impedance matrix of the N-loop network plus its terminations. Equation 4.10 is expanded as follows:

$$e_g[1,0,0...,0]^1 = [Z'][i] = [j\mathbf{M} + s\mathbf{I} + \mathbf{R}][i_1, i_2, i_3, ..., i_N]^t \tag{4.11}$$

where $[\cdot]^t$ denotes matrix ranspose and $\mathbf{I}$ is the unit matrix, $e_g$is the source voltage, and $i_1, i_2, i_3, ..., i_N$ are the currents in each of the N loops of the network.

It is evident that the impedance matrix [z'] is itself the sum of three N x N matrices; 4.3.1, 4.3.2 and 4.3.3 :

4.3.1 Main coupling matrix jM

This is the N x N matrix containing the values of the mutual couplings between the nodes of the network (provided by the transformers in Figure 4.2, and equal in value to the immittance inverters in the lowpass prototype of Figure 4.3). If the coupling is between sequentially numbered nodes, $M_{i,i+1}$, it is referred to as a mainline coupling. The entries on the main diagonal $M_{i,i}(\equiv B_i$, the FIR at each node) are the self-couplings, whereas all the other couplings between the nonsequentially numbered nodes are known as cross-couplings:

$$j\mathbf{M} = j\begin{bmatrix} B_1 & M_{12} & M_{13} & \cdots & M_{1N} \\ M_{12} & B_2 & M_{23} & \cdots & M_{2N} \\ M_{13} & M_{23} & B_3 & \cdots & \vdots \\ \vdots & \vdots & \vdots & \vdots & M_{N-1,N} \\ M_{1N} & M_{2N} & \cdots & M_{N-1,N} & B_N \end{bmatrix} \tag{4.12}$$

Because of the reciprocity of the passive network, $M_{ij} = M_{ji}$, and generally, all the entries are nonzero. In the RF domain, any variation of the coupling values with the frequency (dispersion) may be included at this stage.

4.3.2 Frequency variable matrix sI

This diagonal matrix contains the frequency-variable portion (either the lowpass prototype or the band-pass prototype) of the impedance in each loop, giving rise to an N x N matrix with all entries at zero except for the diagonal filled with $s = j\omega$ as follows:

$$s\mathbf{I} = \begin{bmatrix} 0 & 0 & 0 & \cdots & 0 \\ 0 & s & 0 & \cdots & 0 \\ 0 & 0 & s & \cdots & 0 \\ \vdots & \vdots & \vdots & \vdots & \vdots \\ 0 & 0 & 0 & \cdots & 0 \end{bmatrix} \tag{4.13}$$

4.3.3 Termination impedance matrix R

This N x N matrix contains the values of the source and load impedances in the R_{11} and R_{NN} positions; all the other entries are zero:

$$R = \begin{bmatrix} R_S & 0 & \cdots & 0 \\ 0 & 0 & \cdots & 0 \\ \vdots & \vdots & \ddots & \vdots \\ 0 & 0 & \cdots & R_L \end{bmatrix} \tag{4.14}$$

4.3.4 N x N and N+2 Coupling Matrices

The N x N impedance matrix for the series resonator network are separated out into the matrix's purely reistive and purely reactive parts [equations 4.10 and 4.11] by

$$[z'] = \mathbf{R} + [j\mathbf{M} + s\mathbf{I}] = \mathbf{R} + [z] \tag{4.15}$$

Now, the impedance matrix [z] represents the circuit in Figure 4.5a, a purely reactive network operating between a voltage source with internal impedance R_S and a load R_L.

Typically, the source and load terminations are nonzero, and can be normalized to unity impedance by insertion of impedance inverters M_{S1} and M_{NL} of impedance values $\sqrt{R_S}$ and $\sqrt{R_L}$ respectively, on the source and load side of the network (Figure 4.5). In both cases in Figure 4.5a,b, the impedance as seen looking out from the network on the input side is R_S and on the output side is R_L.

The action of placing the two inverters on either side of the N x N impedance matrix has two effects:

The terminating impedances become terminating conductances $G_S = 1/R_S$ and $G_L = 1/R_L$, respectively, (and also the voltage source e_g is transformed into a current source $i_g = e_g/R_S$).

The [z] matrix surrounded by two inverters can be replaced by the dual network, which is an admittance matrix [y]. The values of the input/output inverters themselves are ten absorbed in the [y] matrix by surrounding the side, creating an N+2 x N+2 matrix, commonly known as the N+2 matrix (Figure 4.5c). The dual of this network, which has series resonators and impedance inverter coupling elements, is illustrated in Figure 4.5d. Whether an impedance or admittance type, the N+2 matrices will have the same values for their mainline and cross-coupling inverters.

The full N+2 network and the corresponding coupling matrix is depicted in Figures 4.6 and 4.7. It can be seen that in addition to the main-line input/output couplings M_{S1} and M_{NL}, it is now possible to include other couplings between the source and/or load terminations, and the internal resonator nodes within the core N x N matrix. Also, it is possible to accommodate the direct source-load coupling M_{SL}in order to realize the fully canonical filter functions. As an admittance matrix, it has parallel resonators and admittance inverters for the coupling elements.

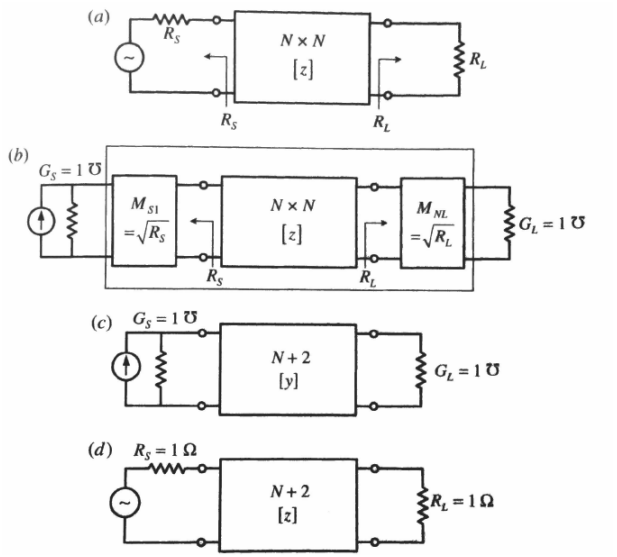

Figure 4.5: Configurations of the input and output circuits for the N x N and N+2 coupling matrices: (a) the series resonator circuit in Figure 4.4 represented as an N x N impedance coupling matrix between terminations R_S and R_L; (b) circuit in (a) with inverters to normalize the terminations to unity; (c) N+2 matrix (parallel resonators) and normalized terminating conductances G_S and G_L; (d) N+2 impedance matrix with series resonators and normalized terminating resistances $R_S$and R_L, the dual network of (c) .

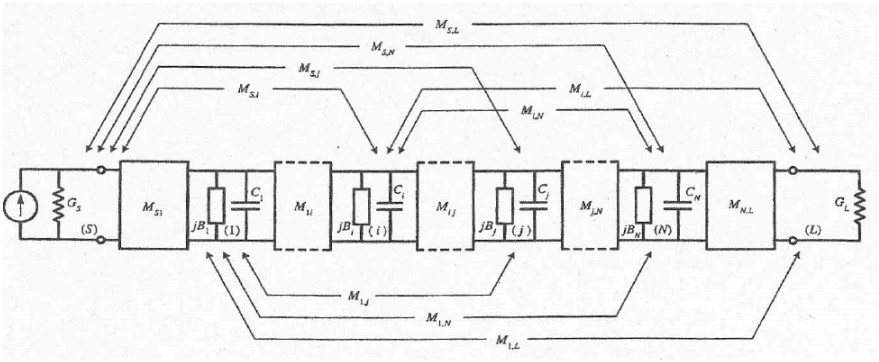

Figure 4.6: N + 2 multicoupled network with parallel lowpass resonators.

	S	1	2	3	4	L
S	M_{SS}	M_{S1}	M_{S2}	M_{S3}	M_{S4}	M_{SL}
1	M_{S1}	M_{11}	M_{12}	M_{13}	M_{14}	M_{1L}
2	M_{S2}	M_{12}	M_{22}	M_{23}	M_{24}	M_{2L}
3	M_{S3}	M_{13}	M_{23}	M_{33}	M_{34}	M_{3L}
4	M_{S4}	M_{14}	M_{24}	M_{34}	M_{44}	M_{4L}
L	M_{SL}	M_{1L}	M_{2L}	M_{3L}	M_{4L}	M_{LL}

Figure 4.7: Fourth-degree N+2 coupling matrix with all possible cross-couplings. The core N x N matrix is indicated within the double lines. The matrix is symmetric about the principal diagonal: i.e. $M_{ij} = M_{ji}$.

4.4 Synthesis of the N+2 Coupling Matrix

In this section, a method is presented for synthesis of the fully canonical or N+2 folded coupling matrix, which overcomes some of the shortcomings of the conventional N x N coupling matrix. The N+2 folded coupling matrix is actually easier to synthesize, has an extra pair of rows, top and bottom, and an extra pair of columns, left and right, surrounding the core N x N coupling matrix, which carry the input and output couplings from the source and load terminations to the resonator nodes in the core matrix.

The N+2 coupling matrix for a filter function is directly created by first synthesizing the coupling matrix for an Nth-degree “transversal” circuit, Figure 4.8, and then reducing this to the folded form, Figure 4.10

shows the folded form node diagram[a].

4.4.1 Synthesis of the Transversal Coupling Matrix

To synthesize the N+2 transversal coupling matrix, we need to construct the two-port short-circuit admittance parameter matrix $[Y_N]$ for the overall network in two ways. First, the matrix is constructed from the coefficients of the rational polynomials of the transfer and reflection scattering parameters $S_{21}(s)$ and $S_{11}(s)$, which represent the characteristics of the filter to be realized, and the second from the circuit elements of the transversal array network. By equating the $[Y_N]$ matrices, derived by these two methods, the elements of the coupling matrix, associated with the transversal array network, are related to the coefficients of the $S_{21}(s)$ and $S_{11}(s)$ polynomials.

4.4.1.1 Synthesis of Admittance Function $[Y_N]$ from the Transfer and Reflection Polynomials

The numerator and denominator polynomials for the $y_{21}(s)$ and $y_{22}(s)$ elements of $[Y_N]$ are built up directly from the transfer and reflection polynomials for $S_{21}(s)$ and $S_{11}(s)$ [equation sets 4.5 and 4.8]. In a doubly terminated network with source and load terminations of 1Ω, it is obtained

For N even:

$$y_{21}(s) = \frac{y_{21n}(s)}{y_d(s)} = \frac{(P(s)/\varepsilon\ )}{m_1(s)}$$
$$y_{21}(s) = \frac{y_{22n}(s)}{y_d(s)} = \frac{n_1(s)}{m_1(s)}$$

For N odd:

$$y_{21}(s) = \frac{y_{21n}(s)}{y_d(s)} = \frac{(P(s)/\varepsilon\ )}{n_1(s)}$$
$$y_{21}(s) = \frac{y_{22n}(s)}{y_d(s)} = \frac{m1(s)}{n_1(s)}$$

where

$$\begin{aligned} m_1(s) &= Re(e_0+f_0) + jIm(e_1+f_1)s + Re(e_2+f_2)s^2 + ... + jIm(e_N+f_N)s^N \\ n_1(s) &= jIm(e_0+f_0) + Re(e_1+f_1)s + jIm(e_2+f_2)s^2 + ... + Re(e_N+f_N)s^N \end{aligned} \tag{4.16}$$

Also, $y_{11}(s)$can be found here, but, like the N x N matrix, it is not needed for synthesis of the N + 2 matrix.

Knowing the denominator and numerator polynomials for $y_{21}(s)$ and $y_{22}(s)$, their residues r_{21k} and r_{22k}, k=1,2...,N may be founded, with partial fraction expansions; and the purely real eigenvalues λ_k of the network found by rooting the denominator polynomial $y_d(s)$, common to both $y_{21}(s)$ and $y_{22}(s)$. The Nth degree polynomial $y_d(s)$ has purely imaginary roots = $j\lambda_k$. Expressing the residues in matrix form yields the following equation for the admittance matrix $[Y_N]$ for the overall network:

[a]White dots are source and load, dark dots are the resonators (8 in this case as the filter of study), continuous bold lines are the main line couplings and dashed lines are the cross couplings.

$$[Y_N] = \begin{bmatrix} y_{11}(s) & y_{12}(s) \\ y_{21}(s) & y_{22}(s) \end{bmatrix} = \frac{1}{y_d(s)} \begin{bmatrix} y_{11n}(s) & y_{12n}(s) \\ y_{21n}(s) & y_{22n}(s) \end{bmatrix} = j \begin{bmatrix} 0 & K_\infty \\ K_\infty & 0 \end{bmatrix} + \sum_{k=1}^{N} \frac{1}{(s - j\lambda_k)} \begin{bmatrix} r_{11k} & r_{12k} \\ r_{21k} & r_{22k} \end{bmatrix} \tag{4.17}$$

Here, the real constant $K_\infty = 0$, except for the fully canonical case where the number of finite-position transmission zeros n_{fz} in the filtering function is equal to the filter degree N. In this case, the degree of the numerator of $y_{21}(s)$ ($y_{21n}(s) = jP(s)/\varepsilon$) is equal to its denominator $y_d(s)$, and K_∞ needs to be extracted from $y_{21}(s)$ first, to reduce the degree of its numerator polynomial $y_{21n}(s)$ by one before its residues r_{21k}can be found. More detail about canonical filters is founded in[4] but it lacks of sense for this project to go in more detail with it.

4.4.1.2 Synthesis of the Admittance Function $[Y_N]$ by the Circuit Approach

In addition, the two-port short-circuit admittance parameter matrix $[Y_N]$ for the overall network can be synthesized directly from the fully canonical transversal network. The general form is depicted in Figure 4.8. The matrix consists of a series of N individual 1st-degree lowpass sections, connected in parallel between the source and load terminations, but not to each other. The direct source-load coupling inverter M_{SL} is included to allow the fully canonical transfer functions to be realized, according to the minimum path rule (i.e.,n_{fzmax}), the maximum number of finite position TZs that can be realized by the network=N-n_{min}, where n_{min} is the number of resonator nodes in the shortest route through the network between the source and load terminations. In fully canonical networks, $n_{min} = 0$, and so $n_{fzmax} = N$, the degree of the network.

Each of the N lowpass sections consists of one parallel-connected capacitor C_k and one frecuency invariant susceptance B_k, connected through admittance inverters f characteristic admittances M_{Sk} and M_{Lk} to the source and load terminations, respectively. The circuit of the kth lowpass section is exhibited in Figure 4.8b.

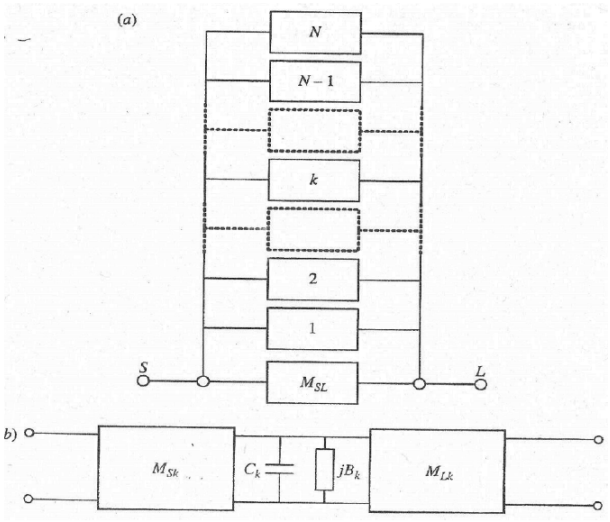

Figure 4.8: Canonical transversal array: (a) N-resonator transversal array including direct source-load coupling M_{SL}; (b) equivalent circuit of the kth lowpass resonator in the transversal array.

4.4.1.3 Synthesis of the Two-Port Admittance Matrix $[Y_N]$

Cascading the elements in Figure 4.8b, $[ABCD]_T = [ABCD]_{M_{SK}}[ABCD]_{C_k}[ABCD]_{b_k}[ABCD]_{M_{LK}}$, gives an [ABCD] transfer matrix for the kth lowpass resonator as follows:

$$[ABCD]_k = -\begin{bmatrix} \frac{M_{Lk}}{M_{Sk}} & \frac{(sC_k+jB_k)}{M_{Sk}M_{Lk}} \\ 0 & \frac{M_{Sk}}{M_{Lk}} \end{bmatrix} \tag{4.18}$$

This is then directly converted into the following equivalent short-circuit y-parameter matrix:

$$[y_k] = \begin{bmatrix} y_{11k}(s) & y_{12k}(s) \\ y_{21k}(s) & y_{22k}(s) \end{bmatrix} = \frac{M_{Sk}M_{Lk}}{(sC_k+jB_k)} \begin{bmatrix} \frac{M_{Sk}}{M_{Lk}} & 1 \\ 1 & \frac{M_{Lk}}{M_{Sk}} \end{bmatrix} = \frac{1}{(sC_k+jB_k)} \begin{bmatrix} M_{Sk}^2 & M_{Sk}M_{Lk} \\ M_{Sk}M_{Lk} & M_{Lk}^2 \end{bmatrix} \tag{4.19}$$

4.4.1.4 Synthesis of the N+2 Transversal Matrix

Now the two expressions for $[Y_N]$, the first in terms of the residues of the transfer function matrix 4.17 and the second in terms of the circuit elements of the transversal array matrix 4.19, can be equated. It is obvious that $M_{SL} = K_\infty$, and for the elements with subscripts 21 and 22 in the matrices in the right-hand sides (RHSs) of equations 4.17 and 4.19, it is obtained

$$\frac{r_{21k}}{(s-j\lambda_k)} = \frac{M_{Sk}M_{Lk}}{(sC_k+jB_k)} \tag{4.20}$$

$$\frac{r_{22k}}{(s-j\lambda_k)} = \frac{M_{Lk}^2}{(sC_k + jB_k)} \tag{4.21}$$

The residues r_{21k} and r_{22k} and te eigenvalues λ_k have already been derived from the $S_{21}$and S_{22} polynomials of the desired filtering function [see equation 4.17], and so by equating the real and imaginary parts in equations 4.20 and 4.21, it is possible to relate them directly to the circuit parameters as

$$\begin{gathered} C_k = 1, \;\; B_k(\equiv M_{kk}) = -\lambda_k \\ M_{Lk}^2 = r_{22k}, \;\; M_{Sk}M_{Lk} = r_{12k} \\ M_{Lk} = \sqrt{r_{22k}} \\ M_{Sk} = r_{21k}/\sqrt{r_{22k}}, \quad \text{k=1,2,...,N} \\ M_{Lk} = r_{12k}/\sqrt{r_{11k}} \\ M_{Sk} = \sqrt{r_{11k}} \end{gathered} \tag{4.22}$$

In conclusion, and numbering the steps for obtaining the N+2 coupling matrix representation of a transversal array circuit from characteristic polynomials :

1. Find A(s), B(s), C(s) and D(s) values with equations 4.5
2. Obtain $[Y_N]$ matrix from [ABCD] one, previous step, and the relations of 4.8
3. Find the residues r_{21k} and r_{22k} and the purely real eigenvalues λ_k from partial fraction expansion of $[Y_N]$, previous step, like showed in 4.17. To obtain the partial fraction expansions Matlab function *residue* is used. This function can be seen implemented in the attached code in APPENDIX B, where rij, Pij and Kij (i,j=1,2) are residues r_{ijk} , eigenvalues λ_k and K_∞ values respectively.
4. Use relations in equations 4.22 to get the values of the transversal coupling network N+2 matrix representation. Matrix in figure 4.9 is obtained.

0	0.2403	0.2403	0.3829	0.3829	0.3549	0.3549	0.3953	0.3953	0
0.2403	-1.1298	0	0	0	0	0	0	0	0.2962
0.2403	0	1.1298	0	0	0	0	0	0	-0.2962
0.3829	0	0	-1.0646	0	0	0	0	0	-0.3258
0.3829	0	0	0	1.0646	0	0	0	0	0.3258
0.3549	0	0	0	0	-0.7477	0	0	0	0.3633
0.3549	0	0	0	0	0	0.7477	0	0	-0.3633
0.3953	0	0	0	0	0	0	-0.2751	0	-0.4045
0.3953	0	0	0	0	0	0	0	0.2751	0.4045
0	0.2962	-0.2962	-0.3258	0.3258	0.3633	-0.3633	-0.4045	0.4045	0

Figure 4.9: N+2 coupling matrix M for the transversal array network of the filter of design.

4.5 Similarity transformations

4.5.1 Reduction of the N+2 Transversal Matrix to the Folded Canonical Form

With N input and output couplings, the transversal topology is clearly impractical to realize for most cases and must be transformed to a more suitable topology. A more convenient form is the folded configuration, Figure 4.10 shows its nodal diagram, realized either directly or as the starting point for further transformations to other topologies that are more appropriate for the technology it is intended to use for the construction of the filter. For this project folded topology will be the starting point to the transformation to cascade quadruplet topology.

To reduce the transversal matrix to the folded form, the formal procedure, described later in this section is applied for the N+2 matrix. This procedure involves a series of similarity transforms (rotations), which eliminate the unwanted coupling matrix entries, alternately , right to left along the rows, and top to bottom down the columns, starting with the outermost rows and columns, and working inward toward the center of the matrix, until the only remaining couplings are those that can be realized by filter resonators in a folded structure, as conveyed in Figure 4.11.

No special action needs to be taken to eliminate the unneeded xa and xs couplings in the cross-diagonals, since they automatically become zero if they are not necessary to realize the particular filter characteristic under consideration.

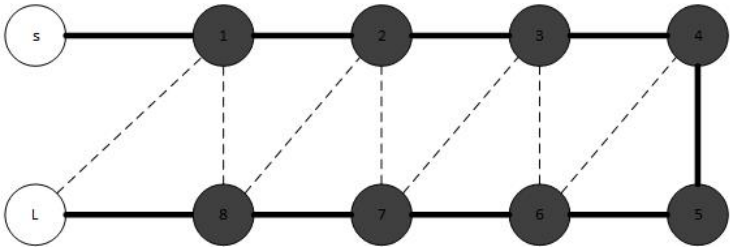

Figure 4.10: Folded N+2 nodal representation of filter of design.

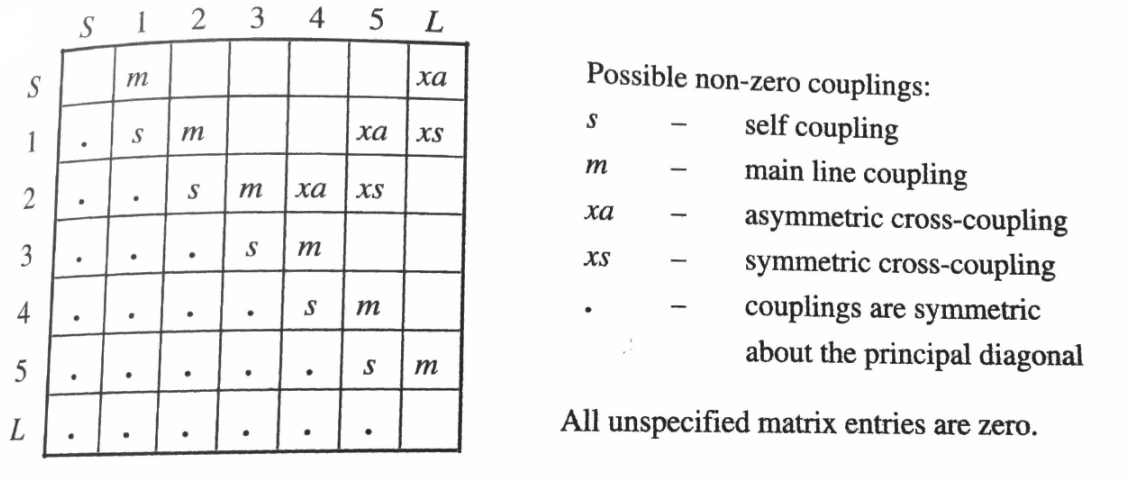

Figure 4.11: Folded coupling matrix form - s and xa couplings are, in general, zero for the symmetric characteristics; couplings are symmetric about the principal diagonal (all unspecified matrix entries are zero).

4.5.1.1 Similarity transformation and Annihilation of Matrix Elements

A similarity transform (or rotation) on an N+2 coupling matrix $\mathbf{M}_0$ is carried out by pre- and postmultiplying $\mathbf{M}_0$ by an N+2 rotation matrix $\mathbf{R}$ and its transpose $\mathbf{R^t}$, from[7]

$$\mathbf{M}_1 = \mathbf{R}_1 \mathbf{M}_0 \mathbf{R}_1^t \tag{4.23}$$

where $\mathbf{M}_0$ is the original matrix, $\mathbf{M}_1$ is the matrix after the transform operation, and the rotation matrix $\mathbf{R}$ is as defined as in matrix 4.24.

Example of seventh-degree rotation matrix $\mathbf{R}_r$, pivot [3,5], and angle θ_r:

$$[R] = \begin{bmatrix} 1 & 0 & 0 & 0 & 0 & 0 & 0 \\ 0 & 1 & 0 & 0 & 0 & 0 & 0 \\ 0 & 0 & c_r & 0 & -s_r & 0 & 0 \\ 0 & 0 & 0 & 1 & 0 & 0 & 0 \\ 0 & 0 & s_r & 0 & c_r & 0 & 0 \\ 0 & 0 & 0 & 0 & 0 & 1 & 0 \\ 0 & 0 & 0 & 0 & 0 & 0 & 1 \end{bmatrix} \tag{4.24}$$

where

$$c_r = R_{ii} = R_{jj} = cos(\theta_r) \qquad s_r = R_{ij} = -R_{ji} = sin(\theta_r)$$

The pivot [i,j] (i≠j) of $\mathbf{R_r}$ indicates that elements $R_{ii}R_{jj} = cos\theta_r$, $R_{ji} = -R_{ij} = sin\theta_r$, (i, j≠1 or N), and θ_r are the angle of the rotation. The other principal diagonal entries are equal to one, and all other off-diagonal entries are zero.

After te transform, the eigenvalues of the matrix $\mathbf{M}_1$ are the same as those of the original matrix $\mathbf{M_0}$, which indicates that an arbitrarily long series of transforms with arbitrarily defined pivots and angles can be applied, starting with $\mathbf{M_0}$.

When a similarity transform of pivot [i,j] and angle θ_r (≠0) is applied to coupling matrix $\mathbf{M}_0$, the elements in rows i and j and columns i and j of the resultant matrix $\mathbf{M}_1$ change, in value, from the corresponding element values in $\mathbf{M}_0$. For the kth element in the row or column i or j of $\mathbf{M}_1$, the value changes according to the following formulas:

$$\begin{aligned} M^1_{ik} &= c_r M^0_{ik} + s_r M^0_{jk} \quad \text{for an element in row i} \\ M^1_{jk} &= c_r M^0_{ik} + s_r M^0_{jk} \quad \text{for an element in row j} \\ M^1_{ki} &= c_r M^0_{ki} - s_r M^0_{kj} \quad \text{for an element in column i} \\ M^1_{kj} &= c_r M^0_{ki} + s_r M^0_{kj} \quad \text{for an element in column j} \end{aligned} \tag{4.25}$$

where k (≠ i,j) = 1,2,3,...N

As explained above, the method for reducing the full coupling matrix $\mathbf{M}_0$ involves applying a series of similarity transforms to the matrix that progressively annihilates the unrealizable or inconvenient elements one by one. The transforms are applied in a certain order and pattern that ensures that once annihilated, an element is not regenerated by a subsequent transform in the sequence. So, unwanted couplings will be eliminated one by one, alternately , right to left along the rows, and top to bottom down the columns, starting with the outermost rows and columns, and working inward toward the center of the matrix, as shown in Figure 4.13 for two first rows and first column, until the only remaining couplings are those that can be realized by filter resonators in a folded structure.

The first element to be annihilated in matrix 4.9 will be M_{S8} (and simultaneously, M_{8S}), a transform of pivot [7,8] and angle $\theta_1 = -tan^{-1}(M_{S8}/M_{S7})$ is applied to the coupling matrix [see the last formula in 4.25 with k=1, i=7, and j=8]. Equation set 4.26 summarizes the angle formulas for annihilating specific elements in the coupling matrix with a rotation at pivot [i,j]:

$$\begin{aligned} \theta_r &= tan^{-1}(M_{ik}/M_{jk}) \quad \text{for } k_{th} \text{ element in row } i\ (M_{ik}) \\ \theta_r &= -tan^{-1}(M_{jk}/M_{ik}) \quad \text{for } k_{th} \text{ element in row } j\ (M_{jk}) \\ \theta_r &= tan^{-1}(M_{ki}/M_{kj}) \quad \text{for } k_{th} \text{ element in column } i\ (M_{ki}) \\ \theta_r &= -tan^{-1}(M_{kj}/M_{ki}) \quad \text{for } k_{th} \text{ element in column } j\ (M_{kj}) \end{aligned} \tag{4.26}$$

Next, the 6 elements in row S, M_{S7},M_{S6},M_{S5},M_{S4},M_{S3} and M_{S2}, are annihilated with transforms at pivots [6,7], [5,6], [4,5], [3,4], [2,3] and [1,2] and angles $-tan^{-1}(M_{S7}/M_{S6})$, $-tan^{-1}(M_{S6}/M_{S5})$, $-tan^{-1}(M_{S5}/M_{S4})$, $-tan^{-1}(M_{S4}/M_{S3})$, $-tan^{-1}(M_{S3}/M_{S2})$ and $-tan^{-1}(M_{S2}/M_{S1})$, respectively [see equation 4.26]. This

transformations leave as a result matrix of Figure 4.12 that also shows in color; which couplings have been annihilated (red) which have to be annihilated (orange) and which have to remain (green) according to Figure 4.10. In blue are shown M_{SL}couplings, that as explained in last section are zero unless it is the canonical case.

Following the same method elements to be annihilated in column L are annihilated and after that, the same will be done with row 1, as it shows in Figure 4.13. Figure 4.14 shows the similarity transform (rotation) sequence for reduction of full coupling matrix to folded form. This sequence can be automatized with a code as the one implemented with Matlab and shown in 6. As it is shown in table of Figure 4.14 and remarking some observations shown below, matrix 4.15 is obtained ;

- The pivot i is chosen always smaller than j.
- Pivots [i,j] are taken as [j-1,j] for M_{kj} and [i,i+1] for M_{ik} annihilation.
- For this order N=8 filter, there are needed r=28 matrix transforms to obtain the folded coupling matrix (Figures 4.10 and 4.15), from the transversal one (Figures 4.8 and 4.9).

0	0.9865	0.0000	0.0000	0.0000	-0.0000	0.0000	0.0000	0.0000	0
0.9865	-0.0000	0.2837	-0.2664	0.4538	-0.3681	0.3052	-0.2271	0.1559	-0.0000
0.0000	0.2837	-1.0586	-0.0669	0.1140	-0.0924	0.0766	-0.0570	0.0392	-0.3054
0.0000	-0.2664	-0.0669	1.0586	0.1214	-0.0985	0.0816	-0.0607	0.0417	0.2867
0.0000	0.4538	0.1140	0.1214	-0.8451	-0.1780	0.1476	-0.1098	0.0754	0.3579
-0.0000	-0.3681	-0.0924	-0.0985	-0.1780	0.8451	0.1819	-0.1354	0.0930	-0.2903
0.0000	0.3052	0.0766	0.0816	0.1476	0.1819	-0.5330	-0.1598	0.1097	-0.4122
0.0000	-0.2271	-0.0570	-0.0607	-0.1098	-0.1354	-0.1598	0.5330	0.1474	0.3068
0.0000	0.1559	0.0392	0.0417	0.0754	0.0930	0.1097	0.1474	0.0000	0.5720
0	-0.0000	-0.3054	0.2867	0.3579	-0.2903	-0.4122	0.3068	0.5720	0

Figure 4.12: First row undesired couplings annihilated.

0	0.9865	-0.0000	-0.0000	-0.0000	-0.0000	0.0000	-0.0000	0.0000	0
0.9865	-0.0000	-0.8136	0.0000	-0.0000	0.0000	0.0000	-0.0000	-0.0000	-0.0000
-0.0000	-0.8136	0.0000	-0.2771	0.3254	-0.3263	0.1801	-0.1347	0.0000	-0.0000
-0.0000	0.0000	-0.2771	0.0000	0.5289	0.5275	-0.3278	-0.4382	-0.5095	-0.0000
-0.0000	-0.0000	0.3254	0.5289	-0.3568	0.0009	-0.0251	-0.4403	-0.3423	0.0000
-0.0000	0.0000	-0.3263	0.5275	0.0009	0.3568	0.4154	0.1496	0.3431	0.0000
0.0000	0.0000	0.1801	-0.3278	-0.0251	0.4154	-0.1293	-0.0381	0.3165	-0.0000
-0.0000	0.0000	-0.1347	-0.4382	-0.4403	0.1496	-0.0381	0.1293	-0.2367	-0.0000
0.0000	-0.0000	0.0000	-0.5095	-0.3423	0.3431	0.3165	-0.2367	-0.0000	0.9895
0	-0.0000	-0.0000	-0.0000	0.0000	0.0000	-0.0000	-0.0000	0.9895	0

Figure 4.13: Second row undesired couplings annihilated.

Transform Number r	Pivot $[i,j]$	Element to be Annihilated	$\theta = c \cdot \tan^{-1}(M_{kl}/M_{mn})$				
			k	l	m	n	c
1	[7,8]	M(S,8)	S	8	S	7	-1
2	[6,7]	M(S,7)	S	7	S	6	-1
3	[5,6]	M(S,6)	S	6	S	5	-1
4	[4,5]	M(S,5)	S	5	S	4	-1
5	[3,4]	M(S,4)	S	4	S	3	-1
6	[2,3]	M(S,3)	S	3	S	2	-1
7	[1,2]	M(S,2)	S	2	S	1	-1
8	[2,3]	M(2,L)	2	L	3	L	1
9	[3,4]	M(3,L)	3	L	4	L	1
10	[4,5]	M(4,L)	4	L	5	L	1
11	[5,6]	M(5,L)	5	L	6	L	1
12	[6,7]	M(6,L)	6	L	7	L	1
13	[7,8]	M(7,L)	7	L	8	L	1
14	[6,7]	M(1,7)	1	7	1	6	-1
15	[5,6]	M(1,6)	1	6	1	5	-1
16	[4,5]	M(1,5)	1	5	1	4	-1
17	[3,4]	M(1,4)	1	4	1	3	-1
18	[2,3]	M(1,3)	1	3	1	2	-1
19	[3,4]	M(3,8)	3	8	4	8	1
20	[4,5]	M(4,8)	4	8	5	8	1
21	[5,6]	M(5,8)	5	8	6	8	1
22	[6,7]	M(6,8)	6	8	7	8	1
23	[5,6]	M(2,6)	2	6	2	5	-1
24	[4,5]	M(2,5)	2	5	2	4	-1
25	[3,4]	M(2,4)	2	4	2	3	-1
26	[4,5]	M(4,7)	4	7	5	7	1
27	[5,6]	M(5,7)	5	7	6	7	1
28	[4,5]	M(3,5)	3	5	3	4	-1

Figure 4.14: Pivotes and angles of rotation used during the transformation of the transversal to the folded coupling matrix.

```
     0    0.9865   -0.0000   -0.0000    0.0000    0.0000    0.0000   -0.0000    0.0000         0
0.9865   -0.0000   -0.8136    0.0000    0.0000    0.0000    0.0000   -0.0000   -0.0000   -0.0000
-0.0000   -0.8136    0.0000   -0.5828   -0.0000    0.0000   -0.0000   -0.0084    0.0000   -0.0000
-0.0000    0.0000   -0.5828    0.0000   -0.5291    0.0000    0.1349   -0.0000    0.0000   -0.0000
 0.0000    0.0000   -0.0000   -0.5291   -0.0000   -0.6633   -0.0000    0.0000   -0.0000   -0.0000
 0.0000    0.0000   -0.0000   -0.0000   -0.6633    0.0000   -0.5435    0.0000   -0.0000    0.0000
 0.0000    0.0000    0.0000    0.1349   -0.0000   -0.5435    0.0000   -0.5990   -0.0000   -0.0000
-0.0000   -0.0000   -0.0084   -0.0000    0.0000   -0.0000   -0.5990    0.0000   -0.8066    0.0000
 0.0000   -0.0000    0.0000    0.0000   -0.0000   -0.0000   -0.0000   -0.8066   -0.0000    0.9895
      0   -0.0000   -0.0000   -0.0000   -0.0000    0.0000   -0.0000    0.0000    0.9895         0
```

Figure 4.15: N+2 coupling matrix M for the folded network of the filter of design.

4.5.2 Reconfiguration of the Folded Coupling Matrix

A direct method for creating a cascade of resonator node quartets is available if the degree of the filter is 8 or higher, and there are two pairs of transmission zeros (each pair realized by one of the two quartets in the cascade[9]). Because the angle of the first rotation is the solution of a quadratic equation, there are restrictions on the pattern of transmission zeros that can be realized. For the cascaded quadruplets (CQ) case, the two zero pairs can lie on the real axis or on the imaginary axis or one pair on each axis. Each

pair must be symmetrically positioned with respect to both axes. CQ nodal diagram representation can be observed in Figure 4.18.

The procedure for synthesizing the pair of quartets needs a series of four rotations to an eighth-degree coupling matrix, starting with the folded configuration. The first rotation angle is obtained by solving a quadratic equation (two solutions), expressed in terms of the coupling elements taken from the original folded coupling matrix

$$t_1^2(M_{27}M_{34}M_{45}-M_{23}M_{56}M_{67}+M_{27}M_{36}M_{56})+t_1(M_{23}M_{36}M_{67}-M_{27}(M_{34}^2-M_{45}^2-M_{56}^2+M_{36}^2))-M_{27}(M_{36}M_{56}+M_{34}M_{45})=0 \tag{4.27}$$

where $t_1 \equiv tan(\theta_1)$. Then, three further rotations are applied according to 4.16 , after which the CQ topology matrix for the 8th-degree filter is obtained as seen in Figure 4.17.

If the minimum path rule is applied to the topology in Figure 4.18, it is obvious that the CQ solution realizes only four TZs in total. Accordingly, the original prototype characteristic should also incorporate only four TZs.

The CQ structure has some practical advantages. One is that the topology can be easily implemented in a dual-mode structure of some kind, and another is that each CQ is responsible for the production of a specific TZ pair, facilitating the development and tuning processes.

Transform number r	Pivot $[i,j]$	Element to be Annihilated	$\theta_r = c \cdot \tan^{-1}(M_{kl}/M_{mn})$				
			k	l	m	n	c
1	[3,5]	-					
2	[4,6]	M_{36}	3	6	3	4	-1
3	[5,7]	M_{27}, M_{47}	4	7	4	5	-1
4	[2,4]	M_{25}	2	5	4	5	+1

Figure 4.16: Pivotes and angles of rotation used during the transformation of the transversal to the folded coupling matrix..

```
     0    0.9865   -0.0000   -0.0000    0.0000    0.0000    0.0000   -0.0000    0.0000         0
0.9865   -0.0000   -0.8032    0.0000    0.1298    0.0000    0.0000   -0.0000   -0.0000   -0.0000
-0.0000  -0.8032    0.0000   -0.6685   -0.0000   -0.0000   -0.0000   -0.0000   -0.0000   -0.0000
-0.0000   0.0000   -0.6685    0.0000   -0.5229    0.0000    0.0000   -0.0000    0.0000   -0.0000
 0.0000   0.1298   -0.0000   -0.5229   -0.0000   -0.5377   -0.0000    0.0000   -0.0000   -0.0000
 0.0000   0.0000   -0.0000    0.0000   -0.5377    0.0000   -0.5442    0.0000    0.0787    0.0000
 0.0000   0.0000   -0.0000   -0.0000   -0.0000   -0.5442   -0.0000   -0.6530   -0.0000   -0.0000
-0.0000  -0.0000    0.0000   -0.0000    0.0000    0.0000   -0.6530    0.0000   -0.8028    0.0000
 0.0000  -0.0000   -0.0000    0.0000   -0.0000    0.0787   -0.0000   -0.8028   -0.0000    0.9895
      0  -0.0000   -0.0000   -0.0000   -0.0000    0.0000   -0.0000    0.0000    0.9895         0
```

Figure 4.17: N+2 coupling matrix M for the cascaded quadruplets network of the filter of design..

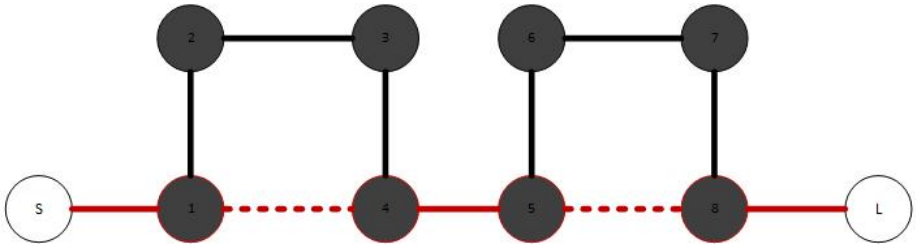

Figure 4.18: Cascade quartet (CQ) configuration with the eighth-order symmetric filtering characteristic, minimum path in red.

Finally, in order to check the efficiency of the matrix obtained, we want to plot the S parameters from this matrix and compare the response with the response obtained from the polynomials.

A normalized N+2 coupling matrix **M** is related to the extracted S-parameters via the following equations

$$S_{21}(s) = 2j[\mathbf{A}]^{-1}_{N+2,1} \tag{4.28}$$

$$S_{11}(s) = -(1+2j[\mathbf{A}]^{-1}_{1,1}) \tag{4.29}$$

where, $\mathbf{A} = -j\mathbf{R} + \omega\mathbf{W} + \mathbf{M}$ is the N+2 immittance matrix for this asymmetric network, **R,** terminal matrix, is a N+2 matrix seen in section 4.14 whose only nonzero entries are $R_{11} = R_{N+2,N+2} = 1$, **W**, frequency matrix, seen in section 4.13 is similar to the N+2 identity matrix, except that $W_{11} = W_{N+2,N+2} = 0$ and ω is the normalized frequency.

So, with equations 4.28 and 4.29 Figure4.19 is obtained. Demonstrating that topology of the network has changed and now the representation of it is with a coupling matrix, but the S-parameters response is still the same as it was with the polynomials.

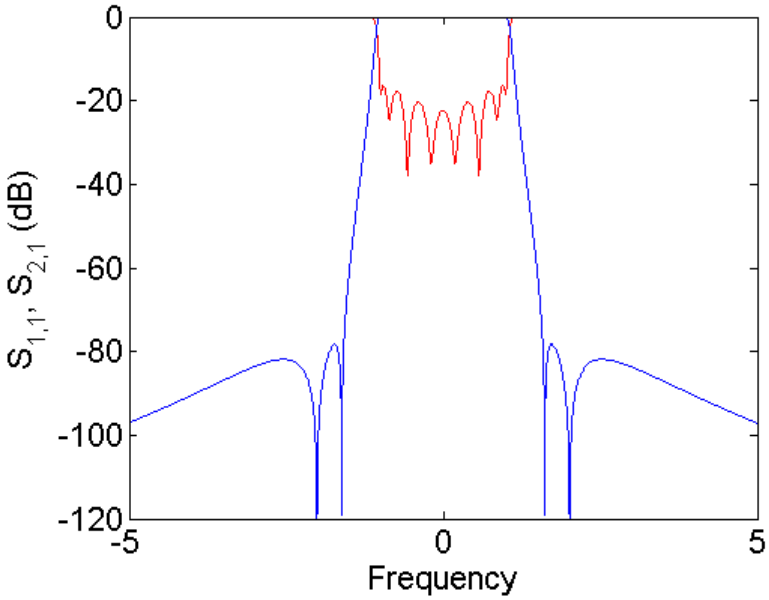

Figure 4.19: Transmission and Reflection parameters obtained with equations 4.28 and 4.28 and from coupling matrix of 4.17.

Chapter 5

PHYSICAL REALIZATION OF THE COUPLING MATRIX

After having obtained the coupling matrix from the filter specification, the next step is to realize it with coupled resonator structure. This part of the process involves the selection of a certain resonator type, the use of coupling mechanisms to provide the desired coupling value between resonators and the implementation of a feed structure. Some of the most important issues related to the practical realization of the filter will be discussed in this chapter.

5.1 General Theory of Couplings

In general, the coupling coefficient of coupled RF/microwave resonators, which can be different in structure and can have different self-resonant frequencies (see Figure 5.1), may be defined on the basis of a ratio of coupled to stored energy

$$k = \frac{\int\int\int \varepsilon \underline{E}_1 \underline{E}_2 \delta v}{\sqrt{\int\int\int \varepsilon |\underline{E}_1|^2 \delta v \ \text{x} \ \int\int\int \varepsilon |\underline{E}_2|^2 \delta v}} + \frac{\int\int\int \mu \underline{H}_1 \underline{H}_2 \delta v}{\sqrt{\int\int\int \mu |\underline{H}_1|^2 \delta v \ \text{x} \ \int\int\int \mu |\underline{H}_2|^2 \delta v}} \tag{5.1}$$

where $\underline{E}$ and $\underline{H}$ represent the electric and magnetic field vectors, respectively; k is the coupling coefficient. Note that, all fields are determined at resonance and the volume integrals are over entire effecting regions with permittivity of ε and permeability of μ. The first term on the right-hand side represents te electric coupling, while the second term represents the magnetic coupling. It should be remarked that the interaction of the coupled resonators is mathematically described by the dot operation of their space vector fields, which allows the coupling to have either positive or negative sign. A positive sign would imply that the coupling enhances the stored energy of uncoupled resonators, whereas a negative sign

would indicate a reduction. Terefore, the electric and magnetic coupling could either have the same effect if they have the same sign, or have the opposite effect if their signs are opposite.

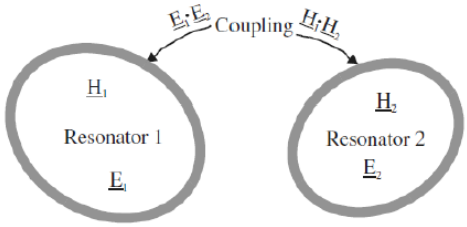

Figure 5.1: General coupled RF/microwave resonators where resonators 1 and 2 can be different in structure and have different resonant frequencies.

5.2 Resonant Cavities

When faced with choice of which type of resonator to use for the structure, there are various options to consider. Although lumped element resonators are today being used at frequencies up to 18 GHz , their attainable unloaded Q-factors vary with frequency. At S-band, lumped element resonators can yield Q-factors of at most a few hundred [10], making it comparable with microstrip resonators. Lumped element resonators have the one major advantage of being smaller than distributed element resonators. However, if high power handling capabilities and low insertion loss are required, one has to make use of high Q (low loss) distributed resonators, like waveguide cavities or coaxial resonator cavities. For resonant frequencies in the low Gigahertz range, the large size of the waveguide cavities required for propagation above cutoff, makes it an unattractive choice. Coaxial resonators are smaller than waveguides resonators of the same frequency, and with unloaded Q-factors in the range of 3000-6000, this implementation is the resonator of choice for the current application. Figure 5.2 shows an example of a coaxial resonator cavity used in the filter realization.

Quarter-wave (λ/4-wave) coaxial resonators are constructed by shorting the center conductor of a coaxial cable to the shield at the far end of the circuit. The length of the cable is exactly λ/4 at the desired resonant frequency. A short circuit is transformed to an open circuit a quarter wavelength away, so when the λ/4-wave coaxial resonator is part of an oscillator circuit, electrically is not even present (Z~∞); however, whenever the frequency of the oscillator attempts to go above or below the resonator's center frequency (due to load changes, temperature changes, etc.), the λ/4-wave section looks like a low impedance that works to attenuate other frequency components. It acts like a parallel tuned L/C tank circuit. The advantage of a λ/4-wave coaxial resonator over a tuned L/C tank circuit is the much higher quality factor, "Q."

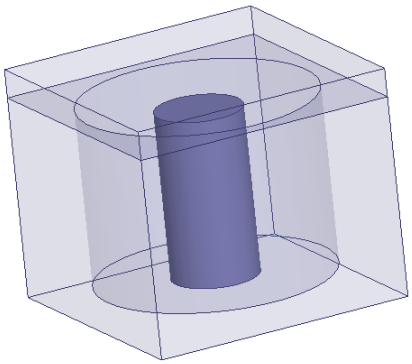

Figure 5.2: A single coaxial resonator post and cavity.

According to [11], a coaxial line has the lowest amount of loss if $\sqrt{\varepsilon_r}Z_0 = 77\Omega$, as also shown in the graph of Figure 5.3 from [12]. For the chosen coaxial resonator realization, the dielectric material is air. Therefore, $\varepsilon_r = 1$, implying an optimal resonator characteristic impedance of 77Ω.

Although the given graphs apply to lines with outside conductors of circular cross section, the assumption is still accurate for coaxial conductors of other shapes.

The choice of which combination of dielectric diameter,D, and conductor diameter,d, to use, is a subject discussed in the following relations and Figure 5.3 ;

Known the quality factor for a cylindrical coaxial resonator we can obtain such relation from its derivative,

$$Q_u = \omega_0 \frac{L}{R} = \omega_0 \frac{\mu}{R_S} \frac{ln(D/d)}{\left(\frac{1}{d}+\frac{1}{D}\right)} = const. \frac{ln(D/d)}{\left(\frac{1}{d}+\frac{1}{D}\right)} \tag{5.2}$$

$$\frac{\delta Q_u}{\delta a} = const. \frac{\left(\frac{-D/d^2}{D/d}\right)\left(\frac{1}{d}+\frac{1}{D}\right) - ln(D/d)\left(-\frac{1}{d^2}\right)}{\left(\frac{1}{d}+\frac{1}{D}\right)^2} = 0 \tag{5.3}$$

$$ln(D/d) - (1+d) = 0 \rightarrow \frac{D}{d} \sim 3.6 \tag{5.4}$$

As it is also seen for a given dominant dimension D, maximum K and hence maximum realizable Qu, $\sqrt{\varepsilon_r}Z_0 = 77\Omega$, is achieved when D/d = 3.6.

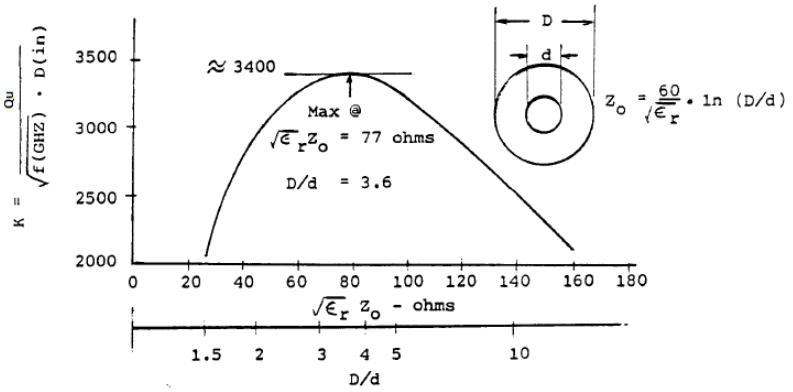

Figure 5.3: Qc of Infinitely Long Coaxial Line.

However, if the geometry is not exactly a cylindrical coaxial, an approximation is can be done between the circle and square areas existing relations. In the end the capability to store electromagnetic energy of the structure is directly linked to the structure's volume.

Knowing the relation between square and circle area,

$$\left.\begin{array}{c} A_{circle} = \pi(D/2)^2 \\ A_{square} = D^2 \end{array}\right\} \frac{A_{circle}}{A_{square}} = \frac{\pi}{4} \rightarrow D_{square\_cavity} = \frac{4}{\pi} D_{circular\_cavity} \tag{5.5}$$

As observed in Figure 5.3 for a cylindrical coaxial resonator Z_0 is given by equation 5.6. For a coaxial line where the external conductor will be a squared prisma instead of a concentric circle, equation 5.7 will be used.

$$Z_0 = \sqrt{\frac{L}{C}} = \frac{1}{v_p C} = \frac{\eta_0}{2\pi\sqrt{\varepsilon_r}} ln(D/d) = \frac{138}{\sqrt{\varepsilon_r}} log_{10}(D/d) = \frac{60}{\sqrt{\varepsilon_r}} ln\left(\frac{D}{d}\right) \tag{5.6}$$

$$Z_0 = \frac{138}{\sqrt{\varepsilon_r}} log_{10}\left(\frac{4}{\pi}\frac{D}{d}\right) \tag{5.7}$$

Figure 5.4 shows a side view and approximate circuit representation of a resonant cavity consisting of a short-circuited transmission line of length l.

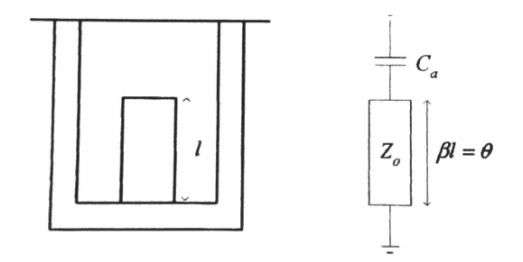

Figure 5.4: Cross section and circuit representation of a single coaxial resonator.

Capacitor C_a represents the total capacitance between the end of the center post and the grounded roof of the cavity. At resonance, the total parallel admittance of the transmission line and capacitor must be zero.

$$\frac{Y_0}{jtan\theta_0} + j\omega_0 C_a = 0 \Rightarrow \; C_a = \frac{1}{Z_0 \omega_0 tan\theta_0} \tag{5.8}$$

In the case where the transmission line is exactly a quarter wavelength long, θ_0 is equal to $\pi/2$, which means that C_a would have to be zero at resonance. This would require an infinite roof height, together with no parasitic capacitance present. For this reason, the length of the resonator is always chosen to be less than a quarter wavelength. Although one can determine the required value of C_a from equation 5.8, there is no simple relation between that value and the distance to the cavity roof. From equation 5.8 it is also clear that the shorter the post length, the bigger C_a has to be at resonance, which means that the distance between the cavity roof and center post is reduced. However, this reduction size comes at the price of a loss in unloaded Q, as the ratio of stored energy to dissipated energy is decreased. For instance, reduction of the cavity roof height from 30mm to 15mm causes the Q-factor to show a substantial decrease of 605.

Additionally, because C_a contains a $1/tan\theta_0$ term, another disadvantage of a smaller cavity (with smaller resonator post length θ_0) is the more rapid variation of the capacitance C_a with θ_0, making the resonant frequency more sensitive to manufacturing tolerances and more difficult to tune than that of a larger cavity. When the roof height is increased from 30mm to 40mm, there is no increase in the Q-factor. So, the best cavity roof height is therefore one which reaches a good compromise between size and unloaded Q.

For the filter of study, post electrical length is $\lambda/8$ instead of $\lambda/4$ ($\pi/2$) this is possible with bigger C_a at expenses of loss in unloaded Q[a].

5.3 External Coupling

For the current implementation, the transformation will be achieved by extending the center conductor of the feed line into the cavity and attaching it to the resonator post at a certain height. As this seems like

[a]In many bandpass filter applications, particularly those applications where the filter is deployed at the front end of a receiver, it is important to know the Qu for the resonators in order to accurately estimate the insertion loss of the filter.

one is 'tapping' into the filter, this type of feed is called a tap point design. An illustration of this feed structure is given in Figure 5.6.

Alteration of the feed position causes the filter response to change. It is, however, possible to optimize the system impedance to a value where the analysis yields the correct response and bandwidth, which means that the external Q-factor has the required value. By repeating this this optimization procedure for various tap positions, it was found that the closer the tap point is place to the short-circuited end of the resonator post, the higher the system impedance has to be for a constant Q_e. This is counter-intuitive, as one would expect the system impedance to decrease as it approaches a short circuit.

The couplings, which connect the filter to the outside world are called external couplings and are often expressed as Q values – that is external Q's. Is the coupling between the I/O connectors and the first/last resonator in the filter. This coupling will be of the type in Figure 5.6, where the centre conductor of the SMA connector is soldered to the resonator ("tapped"), at a certain height above the ground plane. Here, the resonator is coupled to the I/O port by a rod (tapped input) but could also be coupled by, for instance, a non touching capacitive disc, a loop or similar arrangement.

For the tapped resonator in Figure 5.6, the coupling increases by moving the tap-point closer to the top of the resonator. It is also possible to determine the external Q by measuring the group delay of S_{11}.

5.3.1 Group Delay Method

Figure 5.5 shows the equivalent circuit for the first resonator when coupled to the input feed source. The input coupling is represented by the conductance G. The reflection coefficient looking into the single resonator, with respect to a feed line of characteristic admittance G, is given by

$$S_{11} = \frac{G - Y_{in}}{G + Y_{in}} = \frac{1 - Y_{in}/G}{1 + Y_{in}/G} \tag{5.9}$$

The impedance Y_{in} seen looking into the single resonator is

$$Y_{in} = j\omega C + \frac{1}{j\omega L} = j\omega_0 C \left(\frac{\omega}{\omega_0} - \frac{\omega_0}{\omega} \right) \tag{5.10}$$

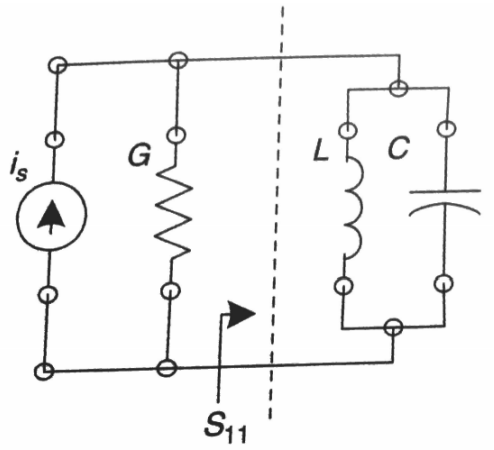

Figure 5.5: Equivalent circuit of the input coupling and first resonator.

where $\omega_0 = 1/\sqrt{LC}$. For frequencies near resonance, $\omega = \omega_0 + \Delta\omega$, where $\Delta\omega \ll \omega_0$, Y_{in} is approximated by

$$Y_{in} \approx j\omega_0 C \frac{2\Delta\omega}{\omega_0} \tag{5.11}$$

Substituting equation 5.11 in the reflection coefficient $S_{11}$of the resonator and noting that $Q_e = (\omega_0 C/G)$, we get

$$S_{11} = \frac{1 - jQ_e(2\Delta\omega/\omega_0)}{1 + jQ_e(2\Delta\omega/\omega_0)} \tag{5.12}$$

The group delay method for determining the input coupling to a single resonator is based analysis of the group delay of the reflection coefficient S_{11}.Equation 5.12 can be rewritten as

$$S_{11} = \left| \frac{1 - jQ_e(2\Delta\omega/\omega_0)}{1 + jQ_e(2\Delta\omega/\omega_0)} \right| \angle\varphi \tag{5.13}$$

where

$$\varphi = -2arctan\left(2Q_e\left(2\frac{(\omega - \omega_0)}{\omega_0}\right)\right) \tag{5.14}$$

Using

$$\frac{\delta}{\delta x}(arctan(x)) = \frac{1}{1+x^2} \tag{5.15}$$

the group delay

$$\tau = -\frac{\delta\varphi}{\delta\omega} \tag{5.16}$$

is also given by

$$\tau = \frac{4Q_e}{\omega_0}\frac{1}{1+(2Q_e(\omega-\omega_0)/\omega_0)^2} \tag{5.17}$$

Note that the group delay has its maximum value at resonance when $\omega = \omega_0$: $\tau_{max} = \tau(\omega_0) = (4Q_e/\omega_0)$ and this leads to equation 5.18.

Simulating we obtain S_{11} parameter in magnitude and phase, phase will be like the one that can be seen in Figure 5.7, from it and using the expressions obtained above, we can obtain Qe (from equation 5.18) and plot it versus the frequency like shown in Figure 5.8.

$$Q_e = \frac{\omega_0\tau}{4} \tag{5.18}$$

Where τ is the group delay from 5.16 where φ , as has been seen is the angle of reflection parameter, Γ, that is .directly equal to the parameter S_{11}.

We make use of markers to identify the maximum value of the group delay and the resonant frequency like in Figure 5.8. We can do this for different tap points, moving the feed line along the lateral side of the resonator and plot the Qe versus the position of the tap point as it can be seen in Figure 5.10. The tap point that fulfills the specification of Qe, equation 5.19, for the desired filter is t=5.5mm.

$$Q_e = \frac{C_i/FBW}{M_{0i}^2} \tag{5.19}$$

Where $C_i = 1F$, FBW is known from 2.3 and $M_{0i} = M_{S1} = M_{L8}$ known from matrix of figure 4.17.

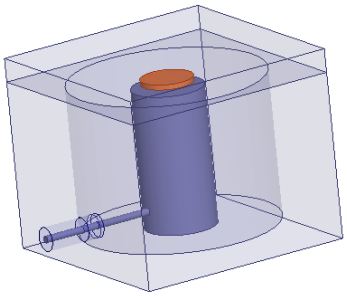

Figure 5.6: Single coaxial cavity resonator with tap point feed line.

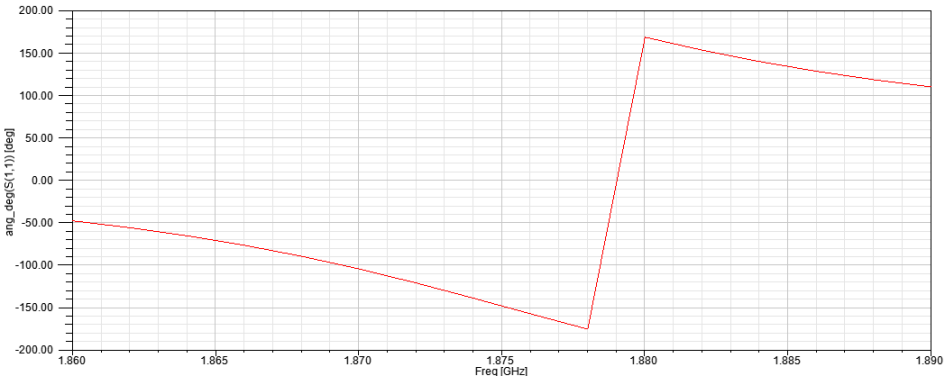

Figure 5.7: S_{11} angle in degrees.

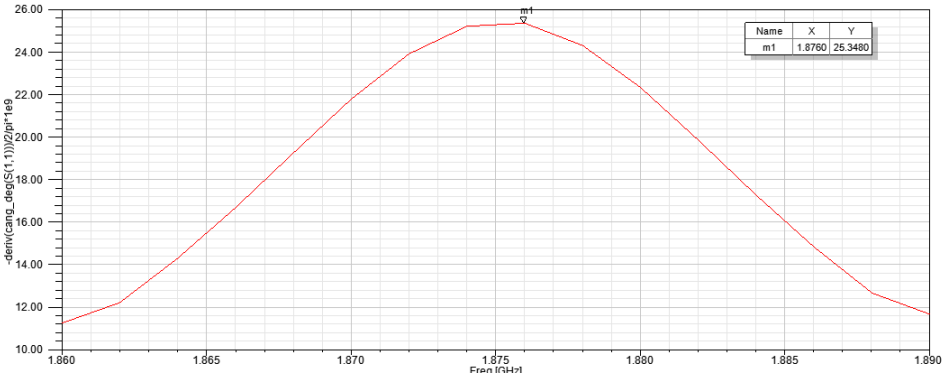

Figure 5.8: External quality factor, Qe, for given tap point and capacitance.

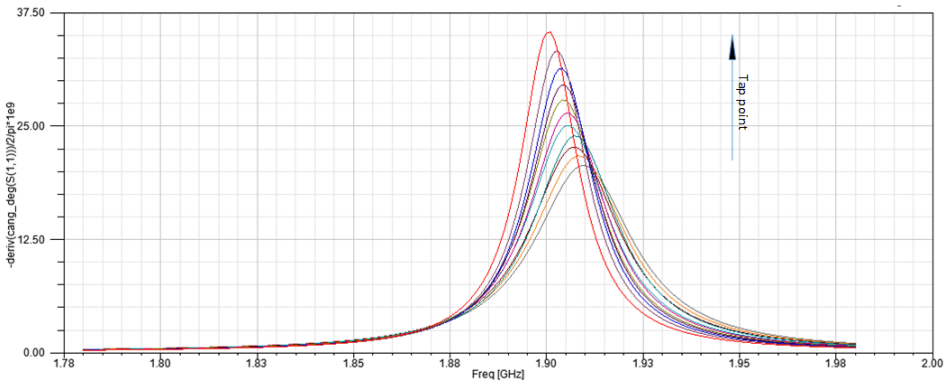

Figure 5.9: Qe with tap point sweep.

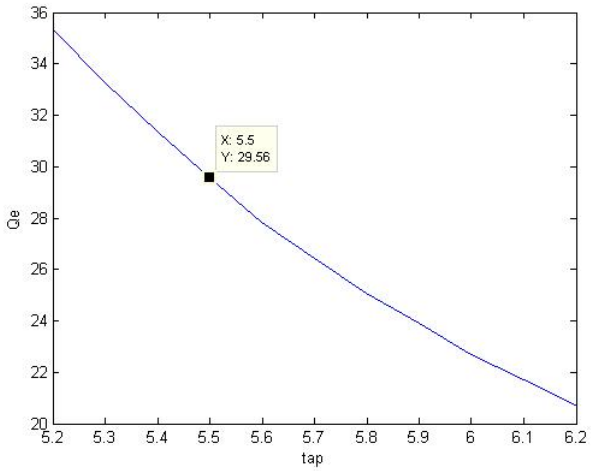

Figure 5.10: Qe vs tap point.

The problem now is that the resonance has been displaced down in frequency, in order to arrange that capacity value must vary experimentally until the desired value is achieved. As it could be seen in Figure 5.9 as tap point increases, Qe decreases but at the same time frequency decreases a little, with the capacitance sweep it can be observed in Figure 5.11 that as capacitance increases frequency decreases but at the same time Qe increases a little.

Figure 5.12[b] shows the needed value of capacitance height of 0.7468 mm, but if the structure is resimulated we could observe how Qe factor has increased a little, so it will be necessary to choose another value of tap point re simulate choose another value of capacitance height as many times as it is wished to fine tune the response and that is very computational time expensive.

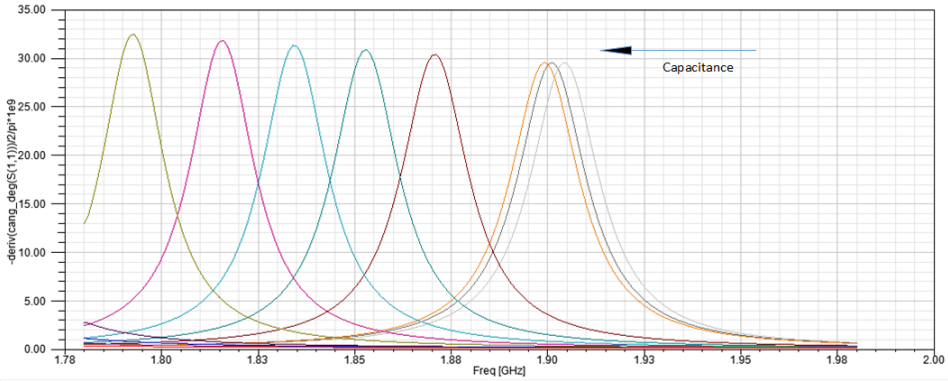

Figure 5.11: Qe with tap point sweep.

[b] In this Figure blue line are measurements and purple line is the Matlab prediction curve based on those measurements. That is useful in order to slightly reduce the number of sweep points in the simulation.

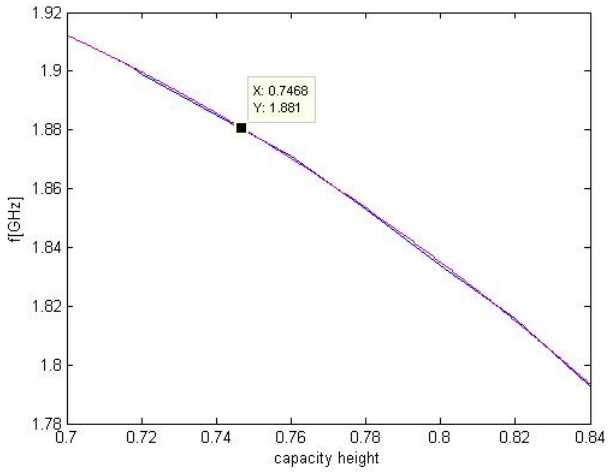

Figure 5.12: Qe with tap point sweep.

5.4 Positive Coupling Mechanisms

There are various ways in which to couple two neighbouring coaxial resonators. The easiest and most obvious way is to cut a hole in the wall which separates the two cavities. This is called iris coupling. Depending on where te iris is positioned, the coupling will be predominantly magnetic, or electric. As the establishment of coupling values is done mainly via simulation, the extraction of coupling values from simulation will be discussed next. Although the theory will be developed for a series coupled LC circuit, it can be applied directly to a parallel coupled circuit, as the same principles are used in the dual parallel derivation.

From [11] the coupling coefficient of a K-inverter between resonators i and j is given by equation

$$k_{ij} = \frac{K_{ij}}{\sqrt{B_i B_j}} \tag{5.20}$$

where B is the reactance slope parameter of the two series resonators and K is the value of the impedance inverter.

$$B = \frac{\omega_0}{2} \left. \frac{\delta\beta(\omega)}{\delta\omega} \right|_{\omega=\omega_0} = \frac{\omega_0}{2} \frac{\delta}{\delta\omega} \left(\omega L - \frac{1}{\omega C} \right)_{\omega=\omega_0} = \omega_0 L \tag{5.21}$$

as at resonance

$$\omega_0 L = \frac{1}{\omega_0 C} \tag{5.22}$$

Also, the value of a K-inverter realized by a T-network of inductors of value M is given by [11]

$$K = \omega M \tag{5.23}$$

By now substituting equations 5.21 and 5.22 into 5.20, the coupling coefficient at resonance is

$$k_{ij} = \frac{M_{ij}}{\sqrt{L_i L_j}} \tag{5.24}$$

For identical resonators,

$$k_{ij} = \frac{M_{ij}}{L} \tag{5.25}$$

The next step in the definition of the coupling factor, is to look at the planes of symmetry utilized by so many analysis methods. Take the simple magnetically coupled two resonator structure of Figure 5.13

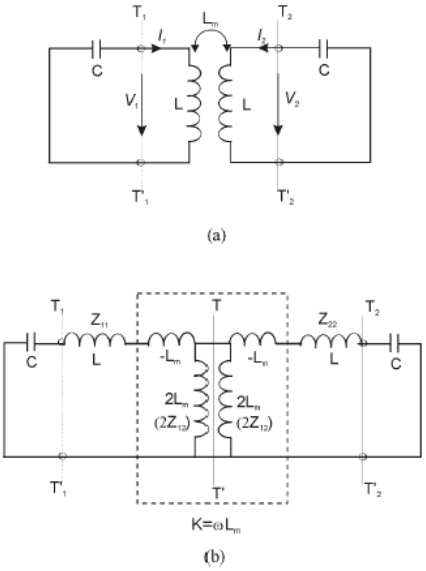

Figure 5.13: (a) Synchronously tuned coupled resonator circuit with magnetic coupling. (b) An alternative form of the equivalent circuit with an impedance inverter $K = \omega L_m$ to represent the coupling.

The introduction of a plane of symmetry makes it possible to determine the resonant frequencies of only half of the structure, first with an electric wall (short circuit) and then with a magnetic wall (open circuit) at the symmetry plane, corresponding to f_e and f_m, respectively.

$$\begin{aligned} f_e &= \frac{1}{2\pi\sqrt{(L-M)C}} \\ f_m &= \frac{1}{2\pi\sqrt{(L+M)C}} \end{aligned} \tag{5.26}$$

By substituting equation 5.25 into equation 5.26 and squaring it, the resonant frequencies can be expressed in terms of the magnetic coupling coefficient k_m.

$$\begin{aligned} f_e^2 &= \frac{1}{4\pi^2(1-k_m)LC} \\ f_m^2 &= \frac{1}{4\pi^2(1+k_m)LC} \end{aligned} \tag{5.27}$$

Therefore,

$$\frac{1}{4\pi^2 LC} = f_e^2(1-k_m) \tag{5.28}$$

and

$$f_m^2 = \frac{(1-k_m)f_e^2}{(1+k_m)} \tag{5.29}$$

It is now possible to solve the coupling coefficient in terms of the electric and magnetic resonant frequencies.

$$k_m = \frac{f_e^2 - f_m^2}{f_e^2 + f_m^2} \tag{5.30}$$

The same procedure can be repeated for two electrically-coupled resonators, as shown in Figure 5.14 L and C form the parallel resonator, with $C_m$the value of the electrical coupling. The result is a coupling coefficient of

$$k_c = \frac{f_m^2 - f_e^2}{f_m^2 + f_e^2} \tag{5.31}$$

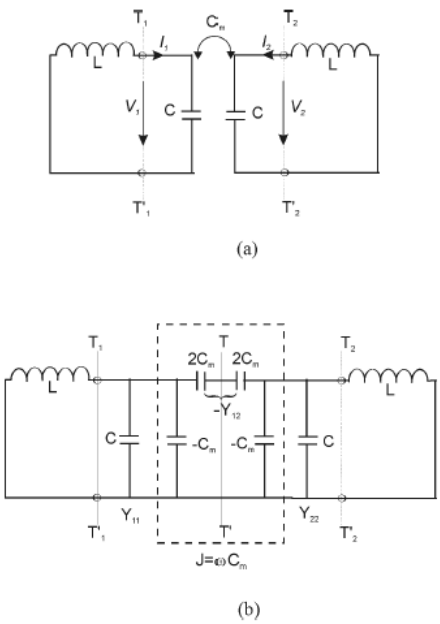

Figure 5.14: (a) Synchronously tuned coupled resonator circuit with electric coupling. (b) An alternative form of te equivalent circuit with an admittance inverter $J = \omega C_m$ to represent the coupling.

Comparison with equation 5.30 shows that the magnetic and electric coupling coefficients differ in sign. It has become common practice to choose magnetic coupling as positive. Therefore, for positive coupling, $f_e > f_m$. In the current implementation, the LC resonators are realized with coaxial cavities. Therefore, when using a simulation software like HFSS, the first establishment of coupling will be through the analysis of two cavities, coupled by an iris of certain size and location. After solving the first two eigenmodes in frequency of the structure and inspecting the field distributions, one finds that one of the modes possesses perpendicular electric fields, while the other mode possesses perpendicular magnetic fields at the plane of symmetry. This corresponds to the introduction of an electric wall (short circuit) and magnetic wall (open circuit), respectively, at the plane of symmetry, see Figure 5.15 . As a result, the frequency of the mode with perpendicular E-fields is f_e, and the frequency of the mode with perpendicular H-fields is f_m, seen in Figure 5.20 . For positive coupling, the eigenmode with perpendicular E-fields at the aperture location should therefore occur at a higher frequency than the eigenmode with perpendicular H-fields. When this is not the case, the coupling is considered negative.

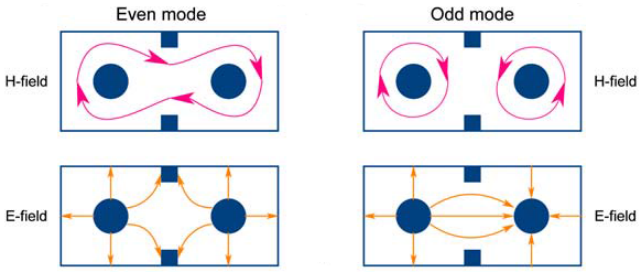

Figure 5.15: H and E fileds representation for even, electric wall, and odd mode, magnetic wall.

The main fields inside a coaxial resonator have the general distribution shown in Figures 5.16 and 5.17.

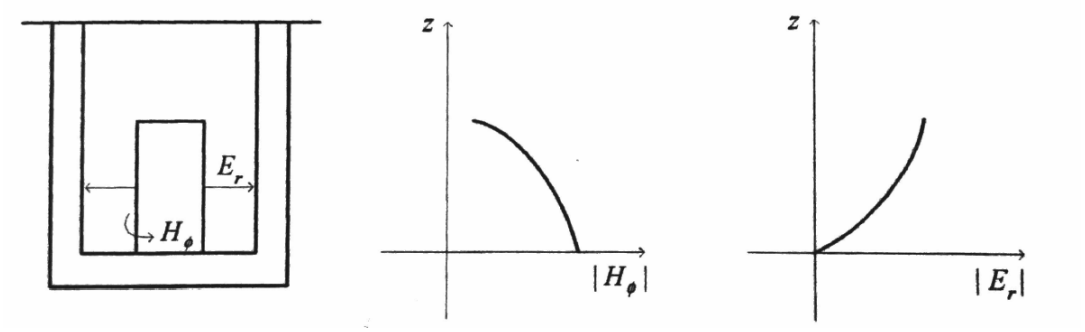

Figure 5.16: General distribution of E-fields and H-fields in a coaxial resonator cavity.

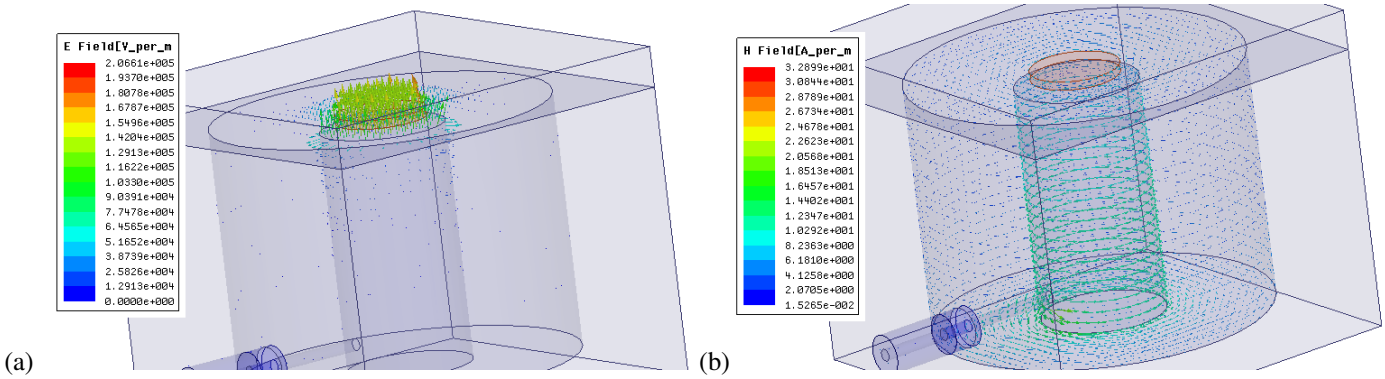

(a) (b)

Figure 5.17: (a) E field simulation. (b) H field simulation.

The radial electric fields are zero at the bottom of the cavity (at z=0) and increase toward the top, while the magnetic fields around the centre post are a maximum at the bottom of the cavity and decrease toward the top.

5.4.1 Inter resonator coupling

To demonstrate the concept of coupling between adjacent resonators the 2- pole circuit in Figure 5.18 is used. Two metallic resonators are enclosed in a metallic housing and loosely coupled to the in- and output ports. Ports are decoupled in order to not influence the coupling, so they have to be far enough to not have influence but close enough to transmit and receive EM energy.

The two resonators are identical[c] and are both resonating at frequency f_0.

To minimize the influence of in- and output connections on the coupling measurement, the resonators must be loosely connected to the input and output ports. If the top-point of the two peaks – or alternatively the "valley" between them - is kept below approximately -30 dB, the influence of the I/O ports can be neglected.

The procedure used here to find the coupling aperture dimensions will be referred to as the "2-pole box" method, and may either be carried out by use of a 3D simulator or experimentally. Vary either the distance - or the aperture opening - between the two resonators and at the same time monitor the resulting coupling bandwidths. In this way, a curve can be made, which shows the relationship between coupling bandwidth and for instance the aperture dimensions. It is clear that this is done most easily in a 3D simulator like HFSS, but if such tools are not available, the 2-pole box may be constructed physically and the coupling bandwidths measured on a network analyzer.

The 2-pole box in Figure 5.18 has two 0.7468 mm tuning screws placed in the lid above the resonators and one 12 mm coupling screw placed in the middle of the aperture opening in the lid. The coupling screw allows tuning of the coupling: The longer the coupling screw goes into the aperture the stronger the positive (inductive) coupling becomes. The coupling screws just above the resonator probe, that are varying C_a, are included in the HFSS model in order to be able to increase or decrease the coupling bandwidth in the final filter. The lengths of the tuning screws are adjusted (and must always have equal lengths) until the two resonance tops, electric and magnetic frequencies, f_e and f_m respectively, are placed symmetrically around f_0 =1.8805 GHz as shown in Figure 5.20. Having obtained those f_m and f_e and applying equation 5.30 we can obtain k_m.

Setting the simulator to do an exhaustive sweep for different iris widths and different screw heights we are able to obtain different k_m and plot it in Figure 5.19, so that for the realization of the next coupling k_{ij}, obtained from equation 5.32, that is needed we can easily relate it to a determined iris width and screw height thanks to this graph

$$k_{ij} = FBW \frac{M_{ij}}{\sqrt{C_i C_j}} \tag{5.32}$$

where $M_{ij}$are the coupling values obtained previously in matrix 4.17 and $C_i$and $C_j$are the lowpass equivalent circuit capacitors and are equal to 1F.

[c]For asynchronous resonators this relation will be used instead of equation 5.30 : $k = \frac{1}{2}\left(\frac{f_{02}}{f_{01}} + \frac{f_{01}}{f_{02}}\right)\sqrt{\left(\frac{f_{p2}^2 - f_{p1}^2}{f_{p1}^2 + f_{p2}^2}\right)^2 - \left(\frac{f_{02}^2 - f_{01}^2}{f_{01}^2 + f_{02}^2}\right)^2}$ where $f_{01}$and f_{02} resonant frequency of independent resonators and $f_{p1}$and f_{p2} resonances of coupled resonators

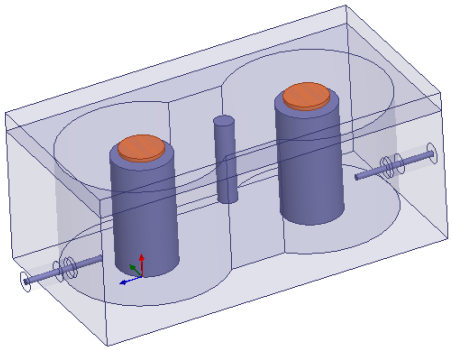

Figure 5.18: Two equal coaxial cavity resonators with magnetic coupling between.

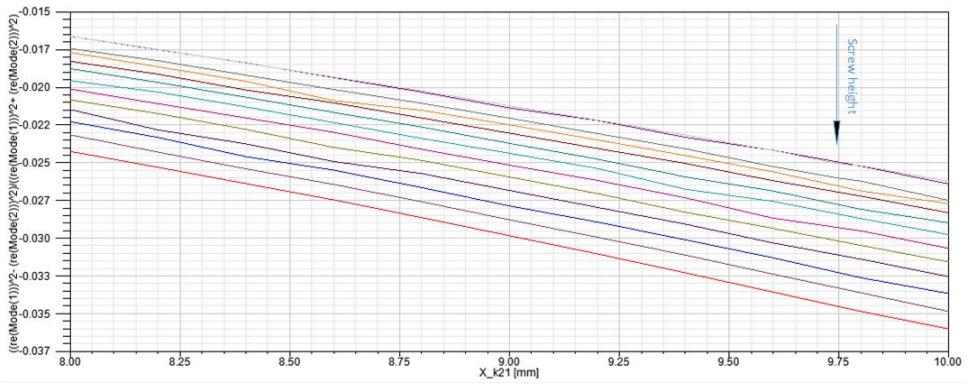

Figure 5.19: Coupling versus iris aperture for different screw lengths.

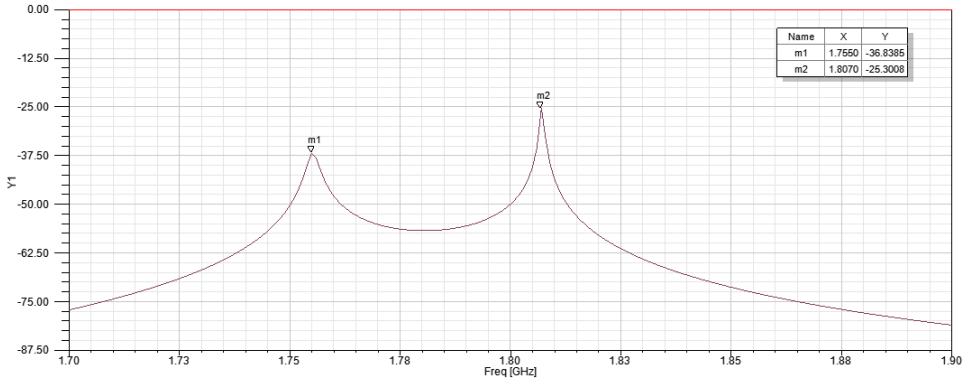

Figure 5.20: Figure 5.18 structureS_{21} parameter.

Finally, it has to be into account that with Figure 5.19 one could deduce that 8.75 mm iris and 12 mm screw will be enough to get the first desired coupling, $k_{12} = -0.0292$, for the filter of design but as it can

be seen in Figure 5.20 and as explained in 5.3.1 there will be a problem of expensive computational time with the fine tuning of capacitances, this time multiplied by two since there are two resonators who affect one with the other.

5.5 Negative Coupling Mechanisms

The achievement of negative coupling between two neighbouring coaxial resonators is no trivial matter. Although the placement of an iris at the open end of the cavity (where the electric fields dominate) can indeed yield negative coupling, these values are small and have a limited range. This poses a problem, as many synthesised values for capacitive coupling require values larger than what iris coupling can provide. Additionally, the dimensions of the structure have a significant effect on the realizability of negative coupling. The three negative coupling mechanisms that are commonly used, explained at[13], include iris-,evanescent mode-and capacitive probe coupling.

For the aim of this project in this section probe coupling will be explained. Figure 5.21 gives an example of two coaxial resonator cavities by a section of transmission line with extended center conductors terminated in circular disks.

This mechanism couples only capacitively (negatively), unlike the iris- and evanescent mode coupling. The price to pay for the large range of negarive coupling, is the extreme sensitivity of the coupling value to the physical parameters, and the relative difficulty with which the structure is manufactured, due to the extension of a thin center conductor and the attachment of small disks at its ends. Additionally, this coupling mechanism is not tunable after its construction.

5.5.1 Cross-coupling

It is well known that couplings between non-adjacent resonators - crosscouplings - may be used either to:

1. Introduce transmission zeroes in the stopband for increased skirt selectivity.

2. Equalize the group delay in the passband.

Couplings may either be inductive or capacitive and are often schematically represented as shown in Figure 4.18 with discontinuous lines. By convention inductive couplings are negative and capacitive couplings positive.

According to Figure 4.17 , a positive (that is capacitive) crosscoupling is needed between cavities 1 and 4 and between cavities 5 and 8.

Coaxial resonators at resonance have high voltages (hence strong electric-fields) near the resonator top and high current density (hence strong magnetic fields) near the bottom. Two such resonators therefore couples capacitively in the top region and magnetically at the bottom region. In the present case positive

coupling may therefore be implemented by an opening in the upper part of the wall, which will allow the electric fields to interact. To "amplify" the capacitive coupling a metallic rod may be suspended in the opening between the resonators. The length of this rod determines the strength of the coupling. In practice the metallic rod is fixed by a PTFE plug or similar dielectric material.

HFSS simulations on the 2-pole box with such small couplings are normally not very accurate. One must therefore be prepared to find the right rod length experimentally once the filter has been manufactured.

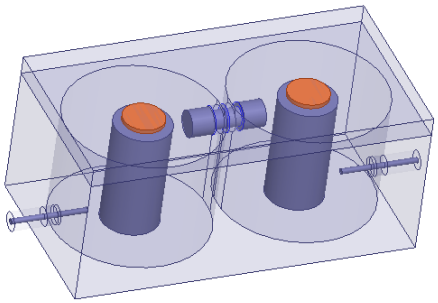

Figure 5.21: Two equal coaxial cavity resonators with electric coupling between.

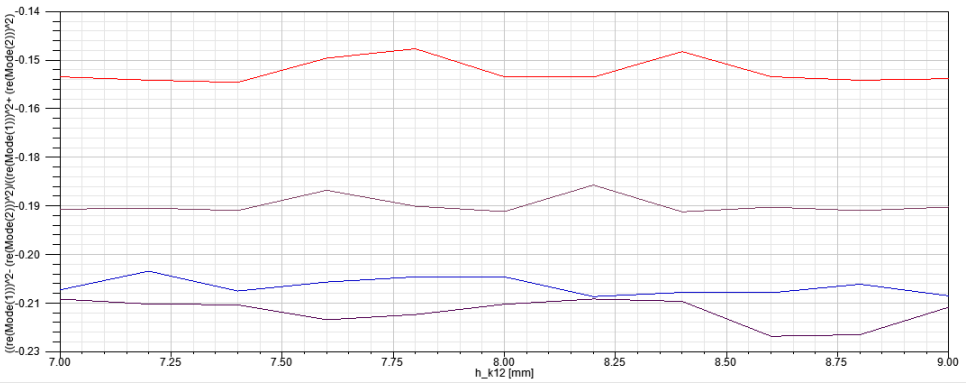

Figure 5.22: Coupling versus cylinder length for different position in heigh.

From extended number of simulations done was observed that larger values of disk radius, however lead to an increase in coupling, due to the greater amount of E-field lines terminating on the disks. Also, the nearer the rod disk to the resonator post, the more the coupling value should increase, this is due to the E-field strength between the disk and the resonator post increases. Figure 5.22 shows one of the sweeps done in height of the rod for different disk radius, but as it can be seen simulations with such small couplings are normally not very accurate

5.6 Filter simulation

5.6.1 High Frequency Structural Simulator (HFSS)

HFSS is a commercial finite element method solver for electromagnetic structures from Ansys. The acronym originally stood for *High Frequency Structural Simulator*. It is one of several commercial tools used for antenna design, and the design of complex RF electronic circuit elements including filters, transmission lines, and packaging.

The power behind HFSS lies in the mathematics of the finite element method (FEM) and the integral, proven automatic adaptive meshing technique. This provides a mesh that is conformal to the 3-D structure and appropriate for the electromagnetic problem you are solving.

In most cases this will be sufficient to provide a good solution, but occasionally it is necessary to assist the mesher when autoadaptative meshing alone is not sufficient.

The normal of a curved surface is different depending on its location, but it is constant for each triangle. (In this context, "normal" is defined as a line perpendicular to the surface). The angular difference between the normal of the curved surface and the corresponding mesh surface is called the normal deviation and is measured in degrees. In Figure 5.23 normal deviation angle representation can be observed, and in Figure 5.24 it can be observed the generated mesh for a normal deviation angle of 10º. That deviation angle is what it has been set for all simulations along this project in order to have a good precision in meshing according to [14].

Figure 5.23: Normal deviation angle representation.

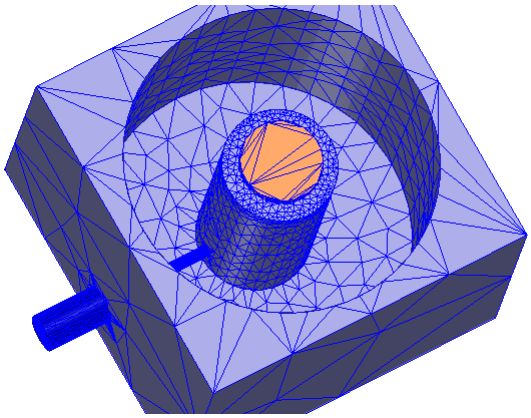

Figure 5.24: Generated mesh in a resonator with 10º maximum normal deviation angle.

Moreover than having into account the mesh that defines the structure created in the simulator, it's important to define the materials, so they will affect in the loses and propagation.

In this filter of study the filter internal walls are silver plated in order to reduce losses because the more intensity in the walls, the more losses will be produced. In other terms, the more wide the center cylinder of the cavity, the more intense the magnetic field so the more intensity in walls and more losses. That's why all dimensions are carefully chosen, even the diameters of the ports to measure follow equation 5.6 to have a 50Ω coaxial line.

5.6.2 WF-00004 Rx Filter HFSS Simulation

Finally the entire filter is constructed in the 3D EM simulator HFSS. First step is to reproduce the exact real filter in the simulator, Figure 5.25, in order to check if similar response with real filter measures, Figure 2.7, are obtained. After a computational expensive simulation, a filter response with deformed passband is obtained. From this model and response a lot of investigation and tests are done and will set the bases for the future lines surrounding this project.

Following methods showed in previous sections in this chapter, every dimension is obtained (iris width, screw lengths, tap point, etc.) and comparing them with the real filter it is found out that are appreciable differences. Simulating the filter with the new dimensions doesn't give a better result. To reduce the number of possible errors, an order 4 filter with 2 placed transmission zeros is designed following all the procedures explained along this project like the order 8, is simulated in HFSS and the result is not what expected. So, to reduce the problem even more, an order 2 Chebyshev filter without induced TZ and 3dB ripple is designed, Figure and simulated in 5.6.2.1. First simulation result was not exactly an accurate result that was expected, but with a sweep in the tapping point gives us a value of tap point that achieves the expected answer, Figure 5.27. So it is observed a difference between the calculated tap point with 5.3.1 and the needed one for the filter, the same way for the 8 order filter design, the tap point was found

out not to coincide with the measured one. The response of the filter is also displaced down in frequency, this is due to capacitances C_a of each resonator has to be adjusted as seen in past sections of this chapter.

In summary the main error sources are:

- C_a *adjustment*; C_a can be adjusted for a pair of resonators, but when another resonator is added it affects the other two and C_a and screws of the three resonators have to be readjusted until a good response is found, with 8 resonators the problem is increased. Dealing with $\lambda/8$ resonators increases the problem, so as explained before another disadvantage of a smaller cavity (with smaller resonator post length θ_0) is a more rapid variation of the capacitance C_a with θ_0. Making the resonant frequency more sensitive to manufacturing tolerances and more difficult to tune than that of a larger cavity. The problem is so extended that it is actually a commercial software that does this adjustment of C_a following the method introduced in [12].
- *Electrical coupling*; HFSS simulations on the 2-pole box with such small couplings are normally not very accurate as has been seen. One must therefore be prepared to find the right rod length experimentally once the filter has been manufactured or find a way to obtain reliable simulation results.
- *Qe variation*; Effects of other resonators, displacement in frequency etc makes tap point slightly vary from calculated value with the simulations and method like shown in section 5.3 and the value obtained when tap point sweep is performed with the whole filter, which is even more computational expensive.

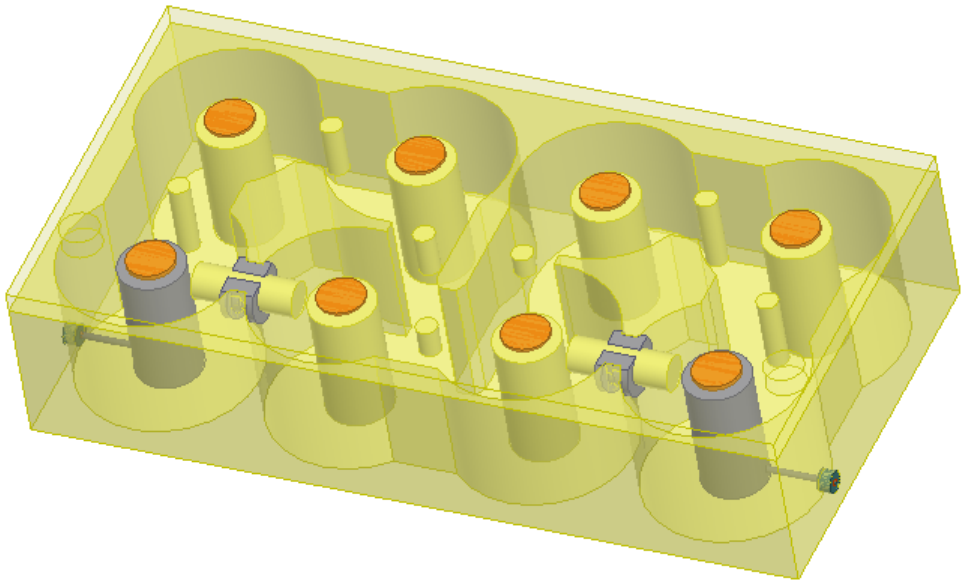

Figure 5.25: WF-00004 PCS Fullband Rx Filter in HFSS.

5.6.2.1 Second order Chebyshev filter with coaxial cavities

As explained in 2.1, Chebyshev response lowpass prototype filter elements are found tabulated. In this simple case, values of lowpass prototype filter elements were extracted from a 3dB ripple (L_{AR}) Chebyshev table (For N=2; g0=1,g1=3.1013,g2=0.5339,g3=5.8095). The coupling values are calculated using

$$k_{i,i+1} = \frac{\Delta f}{f_0} \frac{1}{\sqrt{g_i g_{i+1}}} \tag{5.33}$$

for i=1 to i=n-1. The input and output coupling methods need not be the same as the resonator coupling. However, the input and output coupling must satisfy the relationship

$$Q_e|_{in} = \frac{\beta Z_0}{(J_{0,1})^2} = \frac{g_0 g_1 f_0}{\Delta f} \tag{5.34}$$

and

$$Q_e|_{out} = \frac{\beta Z_0}{(J_{n,n+1})^2} = \frac{g_n g_{n+1} f_0}{\Delta f} \tag{5.35}$$

with 5.3 and 5.4 the values of tap point, iris width and screw height are calculated. Tap point value is found out to be 1mm higher than the calculated one to obtain a decent response.

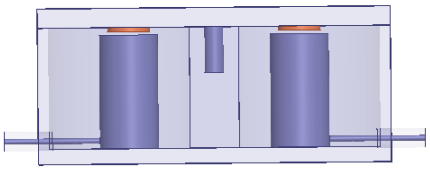

Figure 5.26: Order 2 Chebyshev filter with coaxial resonators.

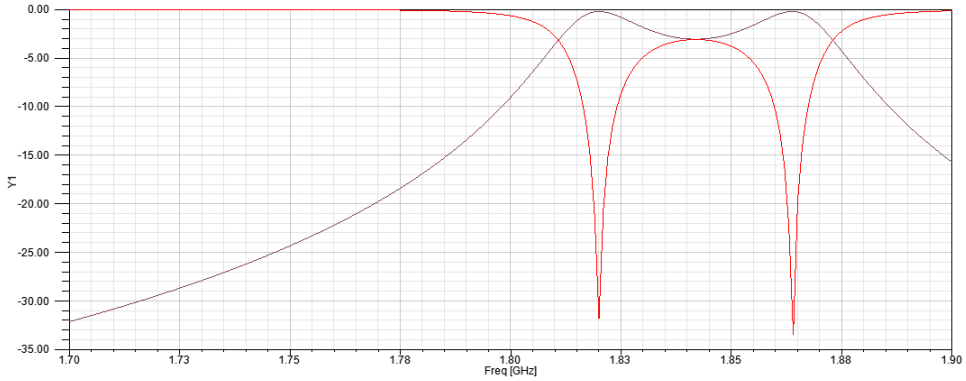

Figure 5.27: Order 2 Chebyshev filter with coaxial resonators transmission and reflection parameters result of HFSS simulation.

Chapter 6

CONCLUSIONS

This project has dealt with the practical aspects of making physical microwave bandpass filters based on coupling matrix synthesis. With the coupling matrix synthesis approach, a set of filter S-parameter characteristics is first created by proper choice of filter order, return loss, unloaded Q and position plus number of transmission zeroes. Then a suitable filter topology is defined and finally the corresponding coupling matrix is synthesized. This coupling matrix fully defines the filter and, with this at hand, the corresponding physical filter can be designed and manufactured. To close the gap between the coupling matrix representation of a filter and the physical filter, practical directions about how to measure/calculate coupling bandwidths and external Q are given. These parameters can be determined by use of 3D EM simulator as the one used in this project, HFSS.

To demonstrate the design process, 8th order coaxial cavity filter for LTE applications between 1.84 and 1.91 GHz have been synthesized using the coupling matrix synthesis method and then compared with the manufactured commercial one, the wf0004 from Lorch. The filter has been synthesized as a cascaded quartet topology with four symmetrically positioned transmission zeroes about the center frequency.

It has been demonstrated then, that polynomial synthesis of a general Chebyshev response can be automatized with the generated code. It has also been demonstrated that coupling matrix synthesis for a cascaded quadruplet topology can be automatized and added to the previous generated polynomial code.

Moreover, following the explained methods iterating with EM simulations and understanding of fields in the coupling of these resonators, filter dimensions were founded and implemented in HFSS. Then compared with exhaustive dimensions measurements of the real filter, finding differences and possible error sources that will define the future work lines.

Future work

- Study of the possible main error sources described in last chapter; C_a adjustment, electrical coupling and Qe variation.

- Extraction of the parasite nodal diagram in order to get a more accurate link between theoretical calculations, EM simulations and real measurements. For instance, the first resonator of a quadruplet is not only coupled to the second, parasitically the EM fields of the first resonator could have an effect on the third.
- Generation of an algorithm for computer aided diagnosis and tuning of this type of microwave filters. Connecting this software with motor arms and network analyzer in order to adjust the screws and process the real time S-parameters response.

REFERENCES

1. D. M. Pozar. *Microwave Engineering, Second Edition*. John Wiley & Sons, inc, 1998.
2. J.-S. HONG. *Microstrip Filters for RF/Microwave Applications*. ohn Wiley & Sons, Inc., 2000.
3. Kenneth V. Puglia. A general design procedure for bandpass filters derived from low pass rototype elements: Part i. MICROWAVE JOURNAL.
4. C. M. Kudsia R. J. Cameron and R. R. Mansour. Microwave filters for communication systems: fundamentals, design, and applications. *Wiley*, 2007.
5. J.D. Rhodes and S.A. Alseyab. The generalized chebyshev low-pass prototype filter. *IEEE Trans. Circuit Theory 8, 113-125*, 1980.
6. R.J. Cameron. Fast generation of chebyshev filter pprototype with asymasymmetric prescribed transmission zeros. *European Space Agency J.6,83-95*, 1982.
7. F.R. Gantmacher. *The Theory of Matrices, Vol.1*. Chelsea Publishing, 1959.
8. A. E. Atia and A. E. Williams. New types of bandpass filters for satellite transponders. *COMSAT Tech. Rev. 1, 21-43*, Fall 1971.
9. R. J. Cameron and J. D. Rhodes. Asymmetric realizations for dual-mode bandpass filters. *IEEE Trans. Microwave Theory Tech. MTT-29, 51-58*, Jan. 1981.
10. R.V. Snyder R. Levy and G Matthaei. Design of microwave filters. *IEEE Trans. on Microwave Theory and Techniques, vol. 50, no. 3, pp. 783-793*, 2002.
11. L. Young G. Matthaei and E.M.T. Jones. *Microwave Filters, Impedance-Matching Networks, and Coupling Structures*. Artech House, 1980.
12. Jr. Daniel G. Swanson. Narrowband combline filter design with ansys hfss. www.swfilterdesign.com.
13. N. Coetzee. *Asymmetric S-Band Coupled Resonator Filters*. PhD thesis, University of Stellenbosch, 2005.
14. Ansoft High Frequency Structure Simulator. Advanced meshing techniques. Training Seminar.
15. R.J. Cameron and J.D. Rhodes. Asymmetric realizations for dual-mode bandpass filters. *IEEE Trans. Microwave Theory Tech. MTT-29, 51-58*, Jan. 1981.

APPENDIX A

APPENDIX A. E(s) polynomial implemented code.

```
function [ Roots, Coeffs] = Es(Proots, Froots, Er, E, even)

syms s

P=1;
for n=1:length(Proots)
    P=P*(s-Proots(n)*1i);
end

F=1;
for n=1:length(Froots)
    F=F*(s-Froots(n)*1i);
end

if even
     Es=(Er*1i*P+E*F);
else
     Es=(Er*P+E*F);
end

Coeffs=sym2poly(Es);
Rootsb = roots(Coeffs);

for n=1:length(Rootsb)
    if real(Rootsb(n))<0
    Roots(n)=real(Rootsb(n))+imag(Rootsb(n))*1i;
    else
```

```
    Roots(n)=-real(Rootsb(n))+imag(Rootsb(n))*1i;
    end
end

d=4;

syms P w;
P=1;
for n=1:length(Roots)
    P=P*(w-Roots(n)/1i);
end

fprintf('E(w)=%s\n',char(vpa(P,d)))
fprintf('E(w)=%s\n',char(vpa(expand(P),d)))

syms P s;
P=1;
for n=1:length(Roots)
    P=P*(s-Roots(n));
end

fprintf('E(s)=%s\n',char(vpa(P,d)))
fprintf('E(s)=%s\n',char(vpa(expand(P),d)))


end
```

APPENDIX B

APPENDIX B. Transversal circuit coupling matrix generation from characteristic polynomials.

```
1
2  N=8;
3  %Characteristic polynomials calculated in previous chapter
4  F=[1 0 2.093 0 1.392 0 0.3054 0 0.01114];
5  Es=[1 1.9462 3.996 4.637 4.645 3.243 1.735 0.6035 0.1113];
6  P= [1i 0 6.6597*1i 0 10.57*1i];
7  e= 93.2344;
8  er=1;
9
10
11 %---[1]---[ABCD] polynomials
12 %A
13 A=zeros(1,length(F));
14 A(1:2:end)=1i*imag(Es(1:2:end)+F(1:2:end)/er);
15 A(2:2:end)=real(Es(2:2:end)+F(2:2:end)/er);
16
17 %B
18 B=zeros(1,length(F));
19 B(1:2:end)=real(Es(1:2:end)+F(1:2:end)/er);
20 B(2:2:end)=1i*imag(Es(2:2:end)+F(2:2:end)/er);
21
22 %C
23 C=zeros(1,length(F));
24 C(1:2:end)=real(Es(1:2:end)-F(1:2:end)/er);
25 C(2:2:end)=1i*imag(Es(2:2:end)-F(2:2:end)/er);
26
27 %D
28 D=zeros(1,length(F));
```

```
D(1:2:end)=1i*imag(Es(1:2:end)-F(1:2:end)/er);
D(2:2:end)=real(Es(2:2:end)-F(2:2:end)/er);


%---[2]---[y] parameters
y11=D;
y12=-1*P/e;
y21=-1*P/e;
y22=A;

%---[3]---admittance parameters expressed as partial fraction
    expansions
[r11,P11,K11]=residue(y11,B);
[r12,P12,K12]=residue(y12,B);
[r21,P21,K21]=residue(y21,B);
[r22,P22,K22]=residue(y22,B);

%---[4]---transversal coupling network matrix realization
    %calculation of couplings
    M_sk=sqrt(r11);
    M_lk=r12./sqrt(r11);
    %creation of the matrix
    M=zeros(N+2);
    %matrix diagonal
    P11=[0; P11; 0];
    M=diag(i*P11,0);
    %Msk values in matrix
    M(1,2:N+1)=M_sk;
    M(2:N+1,1)=M_sk.';
    %Mlk values in matrix
    M(N+2,2:N+1)=M_lk;
    M(2:N+1,N+2)=M_lk.';
```

APPENDIX C

APPENDIX C. Similarity transformations; from transversal topology to folded one.

```
% Coupling matrix: transversal to folded
        for l=N+1:-1:3
            k1=1;
            c=-1;
            Or=c*atan(M(k1,l)/M(k1,l-1));
            R=diag(ones(1,N+2));
            R(l-1,l-1)=cos(Or);
            R(l,l)=cos(Or);
            R(l,l-1)=sin(Or);
            R(l-1,l)=-sin(Or);
            M=R*M*R.';
            real(M)
        end
for I=1:N/2-1
        for k=2+I:N+1-I
            l1=N+3-I;
            c=1;
            Or=c*atan(M(k,l1)/M(k+1,l1));
            R=diag(ones(1,N+2));
            R(k+1,k+1)=cos(Or);
            R(k,k)=cos(Or);
            R(k+1,k)=sin(Or);
            R(k,k+1)=-sin(Or);
            M=R*M*R.';
            real(M)
        end
```

```
29          for  l=N+1-I:-1:3+I
30               k1=1+I;
31               c=-1;
32               Or=c*atan(M(k1,l)/M(k1,l-1));
33               R=diag(ones(1,N+2));
34               R(l-1,l-1)=cos(Or);
35               R(l,l)=cos(Or);
36               R(l,l-1)=sin(Or);
37               R(l-1,l)=-sin(Or);
38               M=R*M*R.';
39               real(M)
40          end
41  end
```

Signed: David Eslava Sabaté

Bellaterra, February of 2016

RESUM

En aquest projecte es tracta la caracterització i modelatge d'un filtre de cavitats mitjançant el simulador electromagnètic 3D HFSS. Partint de les especificacions d'un filtre real de telefonia es realitzarà una caracterització completa, modelat i extracció del diagrama nodal ideal. Per a aconseguir-ho, prèviament s'estudiarà el tipus de resposta a aconseguir i es caracteritzarà amb polinomis. Amb l'enfocament de la matriu d'acoblament, primer un conjunt de característiques dels paràmetres S son creats. Seguidament es defineix una topologia del filtre adecuada i finalment la corresponent matriu d'acoblament és sintetitzada. Aquesta matriu d'acoblament defineix tot el filtre, i , amb això el corresponent filtre físic pot ser dissenyat i fabricat. Per tancar l'intèrval entre la representació de la matriu d'acoblament d'un filtre i el filtre físic, es dónen uns métodes per mesurar/calcular els acoblaments i el Q extern. Aquests paràmetres poden ser determinats amb l'ús d'un simulador EM 3D com l'utilitzat en aquest projecte, HFSS.

RESUMEN

En este proyecto se trata la caracterización y modelado de un filtro de cavidad mediante el simulador electromagnético 3D HFSS. Partiendo de las especificaciones de un filtro real de telefonía se realizará una caracterización completa, modelado y extracción de diagrama nodal ideal. Para ello previamente se estudiará el tipo de respuesta a conseguir y se caracterizará con polinomios. Con el enfoque de la matriz de acoplo, primero un conjunto de características de los parámetros S son creadas. Seguidamente se define una topología del filtro adecuada y finalmente la correspondiente matriz de acoplo es sintetizada. Esta matriz de acoplo define del todo al filtro, y, con esto el correspondiente filtro físico puede ser diseñado y fabricado. Para cerrar el intervalo entre la representación de la matriz de acoplo de un filtro y el filtro físico, se dan unos métodos para medir/calcular los acoplos y el Q externo. Estos parámetros pueden ser determinados con el uso de un simulador EM 3D como el utilizado en este proyecto, HFSS.

ABSTRACT

In this project the characterization of a cavity filter by 3D electromagnetic simulator HFSS is proposed. Based on the specifications of a real cellular filter complete characterization, modeling and ideal nodal diagram extraction will be performed. To do so, previously the kind of response to achieve will be studied and characterized with polynomials. With the coupling matrix synthesis approach, a set of filter S-parameter characteristics is first created. Then a suitable filter topology is defined and finally the corresponding coupling matrix is synthesized. This coupling matrix fully defines the filter and, with this at hand, the corresponding physical filter can be designed and manufactured. To close the gap between the coupling matrix representation of a filter and the physical filter, practical directions about how to measure/calculate coupling bandwidths and external Q are given. These parameters can be determined by use of 3D EM simulator as the one used in this project, HFSS.